9.04 Magma Oceans and Primordial Mantle Differentiation

V Solomatov, Washington University in St. Louis, St. Louis, MO, USA

Nomenclature

A	Surface area of magma ocean
a	Prefactor in nucleation function
a_u	Prefactor in scaling law for velocity
B	Exponential coefficient in nucleation function
c_p	Isobaric specific heat
c'_p	Apparent isobaric specific heat in two-phase regions
D	Diffusion coefficient
d	Crystal diameter
d_crit	Crystal diameter separating equilibrium and fractional crystallization
d_e	Critical crystal diameter for equilibrium crystallization
d_f	Critical crystal diameter for fractional crystallization
d_nucl	Crystal diameter after nucleation
d_ost	Crystal diameter controlled by Ostwald ripening
d'_ost	Crystal diameter at late stages of magma ocean crystallization
E	Activation energy of solid
E_l	Activation energy of melt
f_ϕ	Hindering settling function
F	Heat flux
g	Acceleration due to gravity
G	Gibbs energy
k_B	Boltzmann's constant
l	Mixing length
L	Depth of magma ocean
L'	Depth of shallow magma ocean
M	Mass of magma ocean
n_i	Mole fraction of component i
n_i^l	Mole fraction of component i in liquid
n_i^s	Mole fraction of component i in solid
n_mw	Mole fraction of magnesiowüstite
P	Pressure
Pr	Prandtl number
R	Gas constant

 http://dx.doi.org/10.1016/B978-0-444-53802-4.00155-X

Ra	Rayleigh number
Ra_*	Critical Rayleigh number for transition to no-rotation regime
T	Temperature
$\dot{T}$	Cooling rate
t	Time
T'	Supercooling
Ta	Taylor number
T_{ad}	Adiabatic temperature
t_{conv}	Crystallization time due to solid-state convection
T_e	Effective temperature
T_{liq}	Liquidus temperature
T_m	Magma ocean temperature
t_{ost}	Ostwald ripening time in deep magma ocean
t'_{ost}	Ostwald ripening time in shallow magma ocean
T_{per}	Melting temperature of perovskite
t_{RT}	Rayleigh–Taylor instability time
T_s	Surface temperature
t_s	Settling time
T_{sol}	Solidus temperature
u_0	Amplitude of convective velocity
u_D	Darcy velocity
u_{perc}	Percolation velocity of melt
u_s	Settling velocity of crystals
V	Volume of magma ocean
W	Mechanical work per unit time
x^*	Velocity coefficient for turbulent boundary layer
z	Depth
α	Thermal expansion
α'	Apparent thermal expansion in two-phase regions
α_η	Coefficient in melt fraction-dependent viscosity
δ	Thermal boundary layer thickness
ΔH	Enthalpy change upon melting
ΔS	Entropy change upon melting
ΔS_{per}	Entropy change upon melting of perovskite
ΔT_{rh}	Rheological temperature scale
$\Delta\rho$	Crystal–melt density difference
$\Delta\rho_{RT}$	Density difference for Rayleigh–Taylor instability
ϵ	Efficiency factor
ζ	Ratio of supersaturation to supercooling
η	Viscosity
η_l	Viscosity of melt
η_s	Viscosity of solid
θ	Parameter in analytical solution for nucleation
κ	Coefficient of thermal diffusivity
λ	Aspect ratio of mean flow
μ_i^l	Chemical potential of component i in liquid
μ_i^s	Chemical potential of component i in solid
$\mu_i^l(0)$	Chemical potential of pure component i in liquid state
$\mu_i^s(0)$	Chemical potential of pure component i in solid state
ν	Kinematic viscosity
ρ	Density
σ	Surface energy
σ_{app}	Apparent surface energy
σ_{SB}	Stefan–Boltzmann constant
τ_T	Convective stress scale
τ^*	Skin friction
ϕ	Crystal fraction
ϕ_l	Melt fraction
ϕ_m	Maximum packing fraction
Φ	Energy release per unit time
Ω	Angular velocity

9.04.1 Earth Accretion and the Giant Impact Hypothesis

The idea that the early Earth could have been substantially molten is not new. Lord Kelvin's famous estimate of the age of the Earth was based on the assumption that the Earth was once completely molten and that the present-day surface heat flux resulted from the cooling of the molten Earth (Thomson, 1864). Later, isotopic dating showed that his estimates of the Earth's age were far too short. Radiogenic heating and mantle convection proved to play a major role in the thermal history of the Earth. The assumption of initially molten Earth did not find much observational or theoretical support and was not accepted either. The theory of Earth formation, which dominated in the middle of the twentieth century, was quite the opposite to Lord Kelvin's theory and can be characterized as soft accretion: Earth accreted from a relatively uniform influx of small particles, which gently settled on Earth without causing any 'harm.' Melting, necessary for core formation, was thought to be caused by radiogenic heating later in the Earth's history (Elsasser, 1963).

The first observational evidence that accretion was not so soft came from the Moon. The analysis of samples returned by the Apollo missions suggested a large-scale differentiation of the Moon, which was most easily explained by the crystallization of a lunar magma ocean (Longhi, 1980; Ringwood and Kesson, 1976; Warren, 1985; Wood, 1975; Wood et al., 1970). This led Hostetler and Drake to propose as early as in 1980 that, perhaps, the Earth and other planets were molten in their early histories as well (Hostetler and Drake, 1980).

That Earth accretion was very energetic became obvious upon the realization that the Earth-forming planetesimals also grew with time, like the Earth itself. It was shown that at the latest stages of planetary accretion, the population of Earth-forming planetesimals was very likely to include large bodies. Initially, the largest size was estimated at 10^{-3} of the Earth's mass or about 1000 km in diameter, based on coagulation theory and the observed planetary obliquities, which were assumed to be affected by large impacts (Safronov, 1964, 1978). Numerical investigations showed that the largest impactors could have reached about 0.1 of the Earth's mass, which is equivalent to the size of Mars (Safronov, 1964, 1978; Weidenschilling et al., 1997; Wetherill, 1975, 1985, 1990). Mars-sized impactors had enough energy to melt and partially vaporize the Earth (Benz and Cameron, 1990; Kaula, 1979; Melosh, 1990; Safronov, 1964, 1978).

The giant impact hypothesis suggested a successful explanation for the origin of the Moon, its composition, and the

angular momentum of the Earth–Moon system (Benz et al., 1986, 1987, 1989; Cameron, 1997; Canup, 2004, 2008; Canup and Agnor, 2000; Canup and Asphaug, 2001; Canup and Esposito, 1996; Ida et al., 1997; Newsom and Taylor, 1989; Stevenson, 1987). The conclusion that seems inevitable is that the Earth was born as result of rather 'violent accretion' during which it was substantially melted. An interesting description of this paradigm shift can be found in a short review by Drake (2000).

Although the kinetic energy of giant impacts was undoubtedly the largest energy source, there are other factors that contributed to Earth heating and melting. Numerical models showed that thermal blanketing effects of the atmosphere on the growing Earth helped to retain the heat during the accretion and could have maintained the surface temperature above the solidus (Abe and Matsui, 1986; Hayashi et al., 1979; Matsui and Abe, 1986; Nakazawa et al., 1985; Zahnle et al., 1988). Core formation released energy corresponding to about 2000 K heating of the entire Earth (Flasar and Birch, 1973). Some energy sources were active on a timescale of about $\sim 10^6$ years, which is much shorter than the timescale of planetary formation $\sim 10^7$–10^8 years (Canup and Agnor, 2000; Chambers and Wetherill, 1998; Wetherill, 1990). These include radiogenic heating by short-lived isotopes such as ^{26}Al and ^{60}Fe (Mostefaoui et al., 2005; Shukolyukov and Lugmair, 1993; Srinivasan et al., 1999; Urey, 1955; Yoshino et al., 2003) and electromagnetic induction heating (Sonett et al., 1968). These energy sources contributed to heating and differentiation in both the proto-Earth and the Earth-forming planetesimals during the early stages of planetary formation.

Although the accretion was a stochastic process and the Earth was melted to some degree many times by bodies of varying sizes, the major event was probably the Moon-forming impact at the end of accretion as suggested by numerical simulations (Canup, 2004; Canup and Asphaug, 2001). Such an impact seems to explain best the properties of the Earth–Moon system including its angular momentum, the masses of the Earth and Moon, and the iron depletion of the Moon. After the impact, the mantle temperature varies significantly – from 2000 to 10^4 K, with some parts of the mantle being completely molten and others remaining solid. These estimates are consistent with earlier simulations (Melosh, 1990; Pierazzo et al., 1997; Tonks and Melosh, 1993). Unfortunately, the numerical simulations can look only at the first hours of evolution (1 day at most). It is hard to predict the 'final' temperature distribution – after all major compositional and thermal heterogeneities settle down. This must be a very fast process because the stresses associated with these heterogeneities are huge and might even exceed the ultimate strength of solid rocks, which is of the order of 1–2 GPa (Davies, 1990). The gravitational energy release due to the redistribution of thermal heterogeneities in the mantle and segregation of the remaining iron increases the temperature further by probably another several hundred degrees (Tonks and Melosh, 1990, 1992). Thus, at the end of the large-scale redistribution of density heterogeneities, the hottest mantle material is completely molten, and a small fraction of the coldest material remains solid and accumulate at the bottom of the magma ocean (the solidus temperature at the base of the mantle is around 4000–5000 K; Holland and Ahrens, 1997; Zerr et al., 1998).

Interestingly, Canup's (2004) simulations show that the material that is heated most ($>10^4$ K) is the iron core of the impactor. It quickly sinks into the core of the proto-Earth, thus suggesting that the Earth's core was likely to be very hot. A substantial fraction of the energy of the superheated core is expected to be quickly transferred to the mantle (Ke and Solomatov, 2006, 2009). This may cause an additional melting of the Earth's mantle.

Another important and yet poorly quantified energy source is tidal heating. Given the fact that the Moon was very close to the Earth right after the Moon formation, it is reasonable to expect that tidal heating contributed significantly to sustaining the magma ocean after the Moon-forming event (Sears, 1993; Zahnle et al., 2007).

The term 'magma ocean' has been widely used to describe the initial molten state of the Earth. Originally, this term was applied to the lunar magma ocean and was defined as "a global, near-surface shell of magma, tens or hundreds of kilometers thick" (Warren, 1985). Warren warned about the shortcomings of this term (he proposed a different term, 'magmasphere,' but it is not used as widely as 'magma ocean'): "Among other things, "ocean" implies the system is virtually 100% liquid, with a mainly gas/liquid upper surface and a water-like viscosity of the order of 10^{-2} poise." It has been realized that the structure of the early molten mantle of the Earth and other planets can be quite complex: The molten Earth may have no stable crust in the early times but may develop a thin crust later on while still remaining molten over hundreds of kilometers below the crust; the molten layer may form not only near the surface but also in the middle of the mantle and even at the base of the mantle; and the degree of melting can vary both radially and laterally. Here, we will use the term 'magma ocean' in a broad sense – to describe a partially or a completely molten layer within the Earth's mantle whose motions are controlled largely by liquid viscosity. This means that it can be underground and it can have a relatively large viscosity.

9.04.2 Geochemical Evidence for Magma Ocean

An early global magma ocean would undoubtedly have left some record of its existence in geochemical data. Indeed, early studies showed that segregation of crystals in a deep magma ocean seemed to produce the major element composition of the upper mantle of the Earth (defined by the spinel-perovskite phase transition around 23 GPa) and in particular could explain the elevated Mg/Si ratios in the upper mantle (Agee and Walker, 1988; Herzberg and Gasparik, 1991; Ohtani, 1985; Ohtani and Sawamoto, 1987). However, geochemical models of differentiation of a terrestrial magma ocean showed that any substantial segregation of perovskite crystals in the lower mantle would drive the ratios of minor and trace elements well outside of their observed range (Kato et al., 1988a,b; McFarlane and Drake, 1990; McFarlane et al., 1994; Ringwood, 1990). On the other hand, it was pointed out that the partition coefficients were not well constrained at realistic temperatures, pressures, and compositions of magma oceans and it was premature to draw any conclusions (Presnall et al., 1998). Later studies showed that fractionation of small amounts of Ca-perovskite in addition to Mg-perovskite can increase the allowed amount

of fractionation of perovskite. Possible amounts of perovskite fractionation are in the range from 5% to 15% (Corgne and Wood, 2002; Corgne et al., 2005; Hirose et al., 2004; Liebske et al., 2005a; Walter et al., 2004; Walter and Trønnes, 2004). Ito et al. (2004) suggested that it can be as high as 40%. The third phase, magnesiowüstite (or ferropericlase), does not accommodate trace elements well so that its fractionation is not expected to have any significant effect on elemental ratios (Walter et al., 2004).

The analysis of isotopic data for ^{176}Hf–^{176}Lu and ^{147}Sm–^{143}Nd systems indicates that continental crust formed very early, perhaps in the first 200 million years of evolution, which might require a magma ocean (Albarède et al., 2000; Amelin et al., 1999; Bennett et al., 1993; Bizzarro et al., 2003; Bowring and Housh, 1995; Collerson et al., 1991; Harrison et al., 2005). Isotopic data on compositions of ^{142}Nd produced by short-lived ^{146}Sm (Boyet and Carlson, 2005; Caro et al., 2003) indicate even shorter timescales, within 30 million years, for mantle differentiation.

A simultaneous modeling of several isotopic systems can potentially provide a very tight constraint on mantle differentiation (e.g., Halliday, 2004). Caro et al. (2005) argued that superchondritic Sm/Nd ratios of early Archean rocks can be reconciled with a nearly chondritic Lu/Hf ratio observed in zircons from the same place and of the same age by extraction of about 0.3 wt% of melt from the upper mantle. Differentiation at small degrees of melting was also proposed earlier to explain the ratio of major and minor elements (Gasparik and Drake, 1995).

Another argument for an early molten state of the Earth comes from the fact that core formation on Earth as well as other planetary bodies happened fast, perhaps within 30–50 Myr of the solar system history, which is inferred from the analysis of the short-lived ^{182}Hf–^{182}W system (Foley et al., 2005; Halliday, 2004; Halliday et al., 1996; Jacobsen, 2005; Kleine et al., 2002; Lee and Halliday, 1995; Yin et al., 2002). This requires some degree of melting of the Earth's mantle very early in planetary history (Stevenson, 1990). To what extent the Earth was molten during core formation is not constrained by Hf–W data. The depth of the molten layer of the Earth can be inferred from the analysis of siderophile elements. Laboratory experiments on partition coefficients of siderophile elements suggest that metal/silicate chemical equilibrium was established around 28 GPa and 2200 K, which can be interpreted as the bottom of a magma ocean (Li and Agee, 1996; Righter, 2003, 2011; Righter and Drake, 1997; Righter et al., 1997; Siebert et al., 2012). According to this model, iron delivered by impacts first accumulates at the bottom of a magma ocean and then sinks through the mostly solid layers below the magma ocean (Elsasser, 1963; Karato and Murthy, 1997a,b; Solomatov, 2000; Stevenson, 1981, 1990). The pressure at the bottom of the magma ocean might be noticeably different from the apparent equilibration pressure because metal/silicate equilibrium was established during a 'rainfall' of iron droplets rather than in the iron layer at the base of magma ocean (Rubie et al., 2003). Besides, the bottom of the magma ocean may not be well described as a simple boundary but rather as an extensive partially molten region with variable melt fraction and a complicated structure and dynamics.

The geochemical constraints can be summarized as follows. Only a small amount of perovskite could have been fractionated via crystal–melt segregation (~10%). Chemical differentiation was likely to occur in the upper parts of the mantle via percolation of melt in a partially molten mantle at small melt fractions. The timescales for core formation and mantle differentiation appear to be very close to each other, and both are close to the accretion timescale constrained by numerical simulations (Canup and Agnor, 2000; Chambers and Wetherill, 1998; Wetherill, 1990). This suggests that core formation, mantle differentiation, and accretion might have been occurring simultaneously. The discussion in the succeeding text is based largely on Solomatov and Stevenson (1993a,b,c), Solomatov et al. (1993), and Solomatov (2000).

9.04.3 Thermal Structure of a Convecting Magma Ocean

9.04.3.1 Adiabats

In vigorously convecting systems, such as magma oceans, the temperature distribution is nearly adiabatic and isentropic. In one-phase systems, such as a completely molten or a completely solid layer, the equation for an adiabat is

$$\frac{\mathrm{d}T}{\mathrm{d}P}=\frac{\alpha T}{\rho c_{\mathrm{p}}} \qquad [1]$$

where T is the temperature, P is the pressure, α is the coefficient of thermal expansion, c_{p} is the isobaric specific heat, and ρ is the density.

In two-phase systems, the effects of phase changes need to be considered (Abe, 1993, 1995, 1997; Miller et al., 1991a,b; Solomatov and Stevenson, 1993b). In the absence of chemical differentiation and assuming thermodynamic equilibrium, the volume fractions as well as compositions of each mineral phase depend only on T and p. Thus, the system can be described with the help of two thermodynamic variables, T and p. All thermodynamic parameters such as the coefficient of thermal expansion and the isobaric specific heat can be obtained the same way as for a one-phase system. In terms of two-phase parameters α' and c_{p}', the equation for the adiabat in the temperature range between liquidus and solidus can be written as follows:

$$\frac{\mathrm{d}T}{\mathrm{d}P}=\frac{\alpha' T}{\rho c_{\mathrm{p}}'} \qquad [2]$$

The order-of-magnitude values of α' and c_{p}' are

$$\alpha' \sim \alpha + \frac{\Delta\rho}{\rho\left(T_{\mathrm{liq}}-T_{\mathrm{sol}}\right)} \qquad [3]$$

and

$$c_{\mathrm{p}}' \sim c_{\mathrm{p}} + \frac{\Delta H}{T_{\mathrm{liq}}-T_{\mathrm{sol}}} \qquad [4]$$

where ΔH is the specific enthalpy change upon melting, $\Delta\rho$ is the density difference between solid and liquid, T_{liq} is the liquidus temperature, and T_{sol} the solidus temperature. Usually, the second term dominates, $\alpha' \gg \alpha$, and $c_{\mathrm{p}}' \gg c_{\mathrm{p}}$. Also, α' is affected more strongly than c_{p}' so that the two-phase adiabat is usually steeper than either one-phase adiabat (see Solomatov and Stevenson, 1993b, for the examples when this is not the case). Note that the situation is different for the atmosphere

where the so-called 'wet' adiabat (due to condensation of water) is always less steep than the 'dry' adiabat (e.g., Goody, 1995). Also, because $\alpha' \gg \alpha$ and $c_p' \gg c_p$, the adiabatic gradient, eqn [2], is approximately equal to the Clapeyron slope of the dominant crystallizing phase and the adiabats tend to align with the curves of constant crystal fraction (e.g., solidus and liquidus).

There are several approaches to calculate the adiabats in the magma ocean. The simplest approach is to parameterize the melt fraction as a function of temperature and pressure without considering what phases crystallize and what composition they are (Abe, 1997; Miller et al., 1991a,b). The most rigorous approach would involve building a self-consistent thermodynamic model, which would use the available database for both solid and liquid silicates (e.g., Asimow et al., 1997; Ghiorso, 1997). An intermediate approach is to choose some simple system consisting of only a few components and treat it self-consistently (Solomatov and Stevenson, 1993b).

9.04.3.2 Upper Mantle

Solomatov and Stevenson (1993b) considered two types of three-component systems to describe thermodynamics of the upper mantle. Here, we only consider the eutectic-like system, which seems to be most accurate at low pressures ($P < 10$ GPa). In this system, the three components, olivine, orthopyroxene, and clinopyroxene, are completely insoluble in each other in the solid state. The Gibbs free energy of the system (solid plus melt) is written as

$$G = \sum_{i=1}^{3} \left(n_i^{\mathrm{s}} \mu_i^{\mathrm{s}} + n_i^{\mathrm{l}} \mu_i^{\mathrm{l}} \right) \quad [5]$$

where μ_i^{s} and μ_i^{l} are the chemical potentials of the component i ($i = 1, 2, 3$) in the solid and liquid, respectively, n_i^{s} and n_i^{l} are the mole fractions of the solid and liquid component i, respectively,

$$n_i^{\mathrm{s}} + n_i^{\mathrm{l}} = n_i \quad [6]$$

and n_i is a total mole fraction of the component i in the system:

$$\sum_{i=1}^{3} n_i = 1 \quad [7]$$

The solid phases are assumed to be insoluble in each other. Thus, the chemical potentials of the solid phases are the same as the chemical potentials $\mu_i^{\mathrm{s}(0)}$ of the pure components:

$$\mu_i^{\mathrm{s}} = \mu_i^{\mathrm{s}(0)} \quad [8]$$

The liquid phases are assumed to form ideal solutions:

$$\mu_i^{\mathrm{l}} = \mu_i^{\mathrm{l}(0)} + RT \ln N_i^{\mathrm{l}} \quad [9]$$

where $\mu_i^{\mathrm{l}(0)}$ is the chemical potential of a pure component i in liquid state and N_i^{l} is the mole fraction of the component i in the liquid:

$$N_i^{\mathrm{l}} = \frac{n_i^{\mathrm{l}}}{\sum_{i=1}^{3} n_i^{\mathrm{l}}} \quad [10]$$

The requirement of thermodynamic equilibrium,

$$\mu_i^{\mathrm{l}} = \mu_i^{\mathrm{s}} \quad [11]$$

allows us to uniquely determine the composition of liquid and solid (n_i^{l} and n_i^{s}) and the melt fraction (the mole melt fraction is simply $\sum_{i=1}^{3} n_i^{\mathrm{l}}$) at any given pressure and temperature. All thermodynamic parameters of the combined crystal–melt system, such as the specific heat and the coefficient of thermal expansion, can be calculated from the Gibbs energy using standard thermodynamic relationships.

Figure 1 shows adiabats for this system at $P < 10$ GPa. Variation of melt fraction between liquidus and solidus is given in Figure 2 along with the experimental data from McKenzie and Bickle (1988). The melting temperatures, their gradients, and the fractions of the three components are slightly adjusted to fit the experimental data. Figure 2 shows that the data follow the expected general pattern of an ideal three-component eutectic system. Near the solidus, all three solid phases undergo eutectic melting characterized by a jump in the melt fraction, and one component (clinopyroxene) is completely liquid at the end of eutectic melting. At some melt fraction (around 30%), the slope changes because the second component is completely molten (orthopyroxene). Olivine remains the only solid phase all the way to liquidus.

9.04.3.3 Lower Mantle

The three components in the lower mantle are periclase, MgO; wüstite, FeO; and perovskite, $MgSiO_3$. Perovskite has only a small amount of iron and is considered to be a pure $MgSiO_3$. The system is very similar to the three-component system described earlier for the upper mantle. The main difference is that components 1 and 2 (periclase and wüstite) are assumed to form an ideal solid solution with each other (magnesiowüstite).

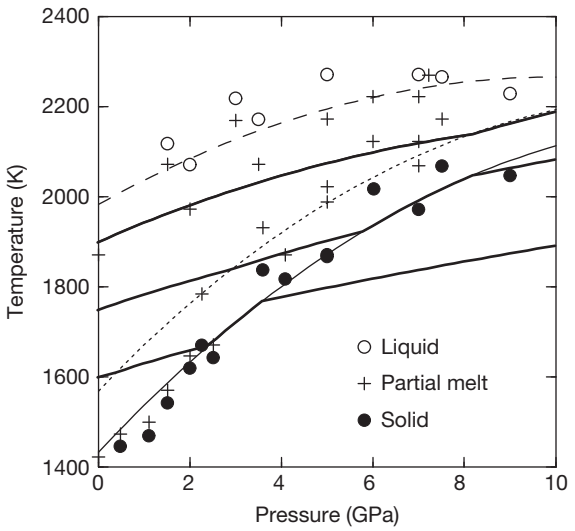

Figure 1 Adiabats in the upper mantle (thick solid lines). Liquidus (dashed line), solidus (solid line), and the beginning of crystallization of orthopyroxene (dotted line) are shown together with experimental data for peridotites (Ito and Takahashi, 1987; McKenzie and Bickle, 1988; Scarfe and Takahashi, 1986). Reproduced from Solomatov VS (2000) Fluid dynamics of a terrestrial magma ocean. In: Canup RM and Righter K (eds.) *Origin of the Earth and Moon*, pp. 323–338. Tuscon, AZ: University of Arizona Press.

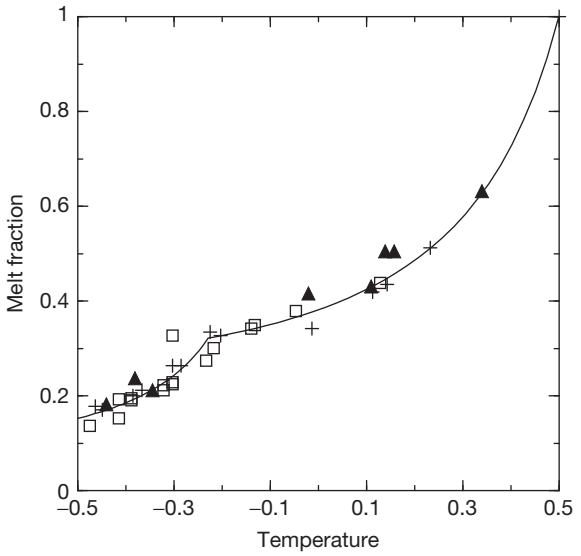

Figure 2 Variation of melt fraction between liquidus ($T=-0.5$) and solidus ($T=0.5$). The experimental data are from McKenzie and Bickle (1988): $0 \le P \le 0.5$ GPa (crosses), $0.5 < P \le 1.5$ GPa (squares), $P > 1.5$ GPa (triangles). The theoretical curve is calculated for an idealized eutectic system consisting of three immiscible components: olivine, orthopyroxene, and clinopyroxene. It shows a typical behavior of this type of systems: a steplike melting at the solidus during which one component – clinopyroxene – melts completely and an abrupt slope change around ~30% melt fraction where the second component – orthopyroxene – melts completely so that only olivine crystals are present until the temperature reaches liquidus. Reproduced from Solomatov VS (2000) Fluid dynamics of a terrestrial magma ocean. In: Canup RM and Righter K (eds.) *Origin of the Earth and Moon*, pp. 323–338. Tuscon, AZ: University of Arizona Press.

Thus, the chemical potentials of the solid phases are described as follows:

$$\mu_i^s = \mu_i^{s(0)} + RT \ln N_i^s, \quad i = 1, 2 \qquad [12]$$

$$\mu_3^s = \mu_3^{s(0)} \qquad [13]$$

where N_i^s is the mole fraction of the component i in the solid:

$$N_i^s = \frac{n_i^s}{\sum_{i=1}^{3} n_i^s} \qquad [14]$$

Figure 3 shows an example of calculations for the lower mantle. The melting temperatures of $MgSiO_3$, MgO, and FeO are based on laboratory experiments and extrapolation to high pressures by Boehler (1992) and Zerr and Boehler (1993, 1994).

The liquidus and solidus curves predicted by this model for the lower mantle are steeper than single phase adiabats. The solidus is very close to the one estimated by Holland and Ahrens (1997) and Zerr et al. (1998). The liquidus T_{liq} approximately follows the melting temperature T_{prv} of pure perovskite $MgSiO_3$ lowered by the presence of MgO and FeO:

$$T_{prv} - T_{liq} \approx \frac{k_B}{\Delta S_{prv}} n_{mw} T_{prv} \qquad [15]$$

where ΔS_{prv} is the entropy change per atom upon melting of pure perovskite and n_{mw} is the mole fraction of magnesiowüstite.

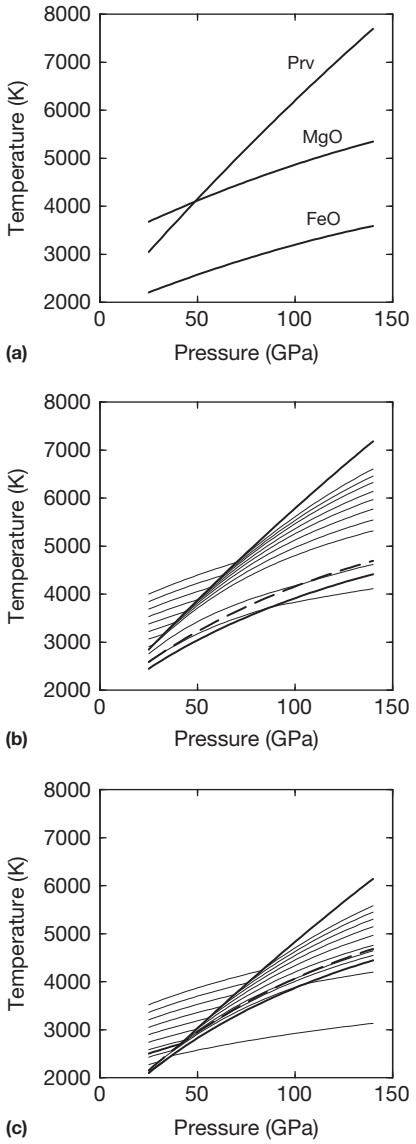

Figure 3 (a) Melting curves of perovskite, MgO and FeO (Boehler, 1992; Zerr and Boehler, 1993, 1994). (b) Adiabats in the convective magma ocean. Liquidus and solidus are shown with heavy solid line. The beginning of magnesiowüstite crystallization is shown with a dashed line. (c) An example of calculations where magnesiowüstite is the first liquidus phase at the top of the lower mantle. Reproduced from Solomatov VS (2000) Fluid dynamics of a terrestrial magma ocean. In: Canup RM and Righter K (eds.) *Origin of the Earth and Moon*, pp. 323–338. Tuscon, AZ: University of Arizona Press.

For $n_{mw} \approx 0.3$, $\Delta S_{prv} \approx 5k_B$ (assuming that the entropy change is approximately k_B per atom, where k_B is Boltzmann's constant; Stishov, 1988) and $T_{prv} \approx 7500$ K (at the base of the mantle), we obtain $T_{prv} - T_{liq} \approx 450$ K. This shows that the liquidus strongly depends on the assumed melting temperature of perovskite. For comparison, Miller et al. (1991a,b) and Solomatov and Stevenson (1993b) assumed a lower melting temperature of perovskite based on the data by Knittle and Jeanloz (1989). The liquidus also depends on the details of the phase diagram. Abe's (1997) lower liquidus is related to his assumption that $MgSiO_3$

and MgO form an ideal solid solution, while in our calculations, perovskite forms eutectic-like subsystems with periclase and wüstite. Recent laboratory experiments and theoretical models significantly refined the thermodynamics of the lower mantle. In particular, they suggest a rather low solidus and liquidus temperatures in the lower mantle and with a relatively small (a few hundred degrees) gap between them at the core–mantle boundary (Andrault et al., 2012; de Koker et al., 2013; de Koker and Stixrude, 2009).

Agee (1990) and Zhang and Herzberg (1994) found that magnesiowüstite is the liquidus phase in both chondrites and peridotites just slightly below the upper mantle/lower mantle boundary. A small fraction of iron in the solid perovskite and the presence of other components (Ca-perovskite) in melt would decrease the liquidus temperature. The estimates of the entropy change are also not very accurate. As a result, magnesiowüstite can be the first liquidus phase at low pressures although at higher pressures, it would still be substituted by perovskite (**Figure 3**).

It is interesting to note that, within the uncertainties of the thermodynamics of the system, crystallization in the lower mantle may not necessarily proceed monotonically from top to bottom. In addition to the crystallizing layer at the surface, an additional layer may form somewhere in the middle of the lower mantle propagating both upward and downward (Mosenfelder et al., 2009; Solomatov and Stevenson, 1993b; Thomas et al., 2012). In combination with crystal–melt density inversion, this may lead to the formation of more than one long-lived partially molten layers at the end of magma ocean crystallization (see also **Section 9.04.9.5**).

9.04.4 Viscosity of the Magma Ocean

Viscosity is an important parameter that controls virtually all dynamic processes in the magma ocean and affects the outcome of crystallization of the magma ocean. The viscosity of the magma ocean varies in a very broad range.

At low degrees of melting, the viscosity of peridotitic magmas can be quite high, on the order of 100 Pa s (Kushiro, 1980, 1986). This is related to relatively low temperature as well as relatively felsic composition – the large concentration of silicon in the initial melts tends to increase the viscosity. The viscosity decreases with temperature very rapidly. Experimental and theoretical studies suggest that the viscosity of many near-liquidus ultramafic silicates at low pressures is around $\eta_l \sim 0.1$ Pa s (Bottinga et al., 1995; Bottinga and Weill, 1972; Dingwell et al., 2004; Liebske et al., 2005b; Persikov et al., 1997; Shaw, 1972).

There are no experimental data for the viscosity of the lower mantle. The viscosity behaves nonmonotonically with pressure because of the structural changes in the polymerized melts (e.g., Kushiro, 1980; Poe et al., 1997). The viscosity of a completely depolymerized melt weakly increases with pressure (Andrade, 1952; Gans, 1972). An increase of less than one order of magnitude can be expected along the liquidus throughout the lower mantle. Thus, the viscosity of magma oceans near the liquidus is probably around 10^{-1} Pa s. In the region between solidus and liquidus, the viscosity of pure melt (without crystals) is somewhat higher because of the lower temperatures. However, the temperature effect is small for low-viscosity liquids (<1 Pa s), which exhibit a power law rather than Arrhenius behavior (Bottinga et al., 1995; Liebske et al., 2005b). First-principles molecular dynamics simulations give similar results (Adjaoud et al., 2012; Karki and Stixrude, 2010). The value of 10^{-1} Pa s with the uncertainty of a factor of 10 will be assumed for the upper mantle as well as for the lower mantle (**Table 1**).

Many authors pointed out that magma oceans can contain substantial amounts of water (Abe et al., 2000; Ahrens, 1992; Righter et al., 1997). Although water reduces the viscosity of magmas, in the limit of high temperatures, the viscosities and diffusivities of many liquids including water are very similar (Persikov et al., 1997). Therefore, the viscosity of completely depolymerized, high-temperature hydrous magma is unlikely to be much different from that of anhydrous magma.

The most important effect on magma viscosity is the presence of crystals. The viscosity of a crystal–melt mixture changes relatively little with the solid fraction. At small volume fraction ϕ of solids, the viscosity η of the mixture can approximately be described with the help of Einstein's linear formula for diluted suspensions of perfectly spherical particles (Einstein, 1906):

$$\eta = \eta_l(1 + 2.5\phi) \quad [16]$$

Various formulas have been proposed to describe the viscosity of suspensions at large crystal fractions (Brinkman, 1952; Campbell and Forgacs, 1990; Costa, 2005; Frankel and Acrivos, 1967; Krieger and Dougherty, 1959; McBirney and Murase, 1984; Mooney, 1951; Murray, 1965; Roscoe, 1952). For example, one of the most popular expressions is (Roscoe, 1952)

$$\eta = \frac{\eta_l}{(1 - \phi/\phi_m)^{2.5}} \quad [17]$$

where ϕ_m is the maximum packing crystal fraction.

Although the previous equation does not describe the viscosity accurately near $\phi = \phi_m$, it does show an important physical aspect of solid/liquid mixtures, that is, the viscosity becomes

Table 1 Typical parameters of a deep magma ocean

Density, ρ	4×10^3	kg m^{-3}
Temperature, T	4×10^3	K
Thermal expansion, α	5×10^{-5}	K^{-1}
Thermal capacity, c_p	10^3	J kg^{-1} K^{-1}
Gravity, g	10	m s^{-2}
Crystal–melt density difference, $\Delta\rho$	300	kg m^{-3}
Viscosity of melt at liquidus, η_l	0.1	Pa s
Viscosity of solids at solidus, η_s	10^{18}	Pa s
Diffusion coefficient, D	10^{-9}	m^2 s^{-1}
Enthalpy change upon melting, $\Delta H\rho$	10^6	J kg^{-1}
Surface energy, σ	0.5	J m^{-2}
Apparent surface energy, σ_{app}	0.02	J m^{-2}
Liquidus gradient, dT_{liq}/dz	2×10^{-3}	K m^{-1}
Adiabatic gradient, dT_{ad}/dz	6×10^{-4}	K m^{-1}
Heat flux, F	10^6	J m^{-2} s^{-1}
Angular velocity, Ω	10^{-4}	s^{-1}
Magma ocean depth, L	3×10^6	m
Remaining molten layer depth, L'	5×10^5	m
Convective velocity, u_0	10	m s^{-1}
Timescale for Ostwald ripening, t_{ost}	10^6	s
Effective cooling rate in plumes, $\dot{T}$	0.2	K s^{-1}
Nucleation prefactor, a	10^{20}	m^{-3} s^{-1}
Crystal size, d	10^{-3}	m

infinite when the crystal fraction reaches ϕ_m. The deformation beyond $\phi = \phi_m$ is only possible if crystals deform via solid-state creep, which is many orders of magnitude slower.

The value of ϕ_m for ideal spheres is around 0.64. For a binary mixture in which the small spheres have just the right size to fit the space in between large spheres (about 30% smaller than the large spheres), $\phi_m = 0.86$ (McGeary, 1961). In reality, the crystal distribution is far from any hypothetical one. Moreover, the shape of crystals is not spherical. Saar et al. (2001) showed that crystal network can form at crystal fraction as low as 10% or 20% depending on the elongation (the smaller number is for a rather large ratio of the longest side of the crystal to the shortest one – over a factor of 10). In the presence of shear, the elongation can affect ϕ_m in the opposite direction. Elongated crystals can align with the flow and develop a hydrodense suspension with as much as 80% crystal fraction (Nicolas and Ildefonse, 1996).

The experiments on partial melts provide the most direct constraint on magma viscosity and ϕ_m, although the melt composition is still different from that of the magma ocean. These experiments show a rapid increase of the viscosity at high crystal fractions and $\phi_m \approx 60\%$ (Arzi, 1978; Lejeune and Richet, 1995; van der Molen and Paterson, 1979). The value of ϕ_m in the experiments is determined from a theoretical fit using equations similar to eqn [17].

Complications arise due to crystal–crystal interactions in the vicinity of ϕ_m. They are most likely to be responsible for the non-Newtonian behavior of partial melts characterized by substantial yield strength (reported values range from 10^2 to 10^6 Pa) and nonlinear relationship between stress and strain rate (Lejeune and Richet, 1995; McBirney and Murase, 1984; Pinkerton and Sparks, 1978; Robson, 1967; Ryerson et al., 1988; Shaw, 1969; Shaw et al., 1968).

The transition from fluidlike behavior to solid-like behavior occurs in a rather narrow range of crystal fraction. Thus, it can be called the 'rheological transition.' At ϕ only slightly smaller than ϕ_m, the viscosity is not much different from that of a pure melt except for corrections described by eqns [16] and [17]. At $\phi > \phi_m$, the deformation rate is controlled by the viscosity of the solid matrix reduced by the presence of melt (Cooper and Kohlstedt, 1986; Hirth and Kohlstedt, 1995a,b; Jin et al., 1994; Kohlstedt and Zimmerman, 1996; Mei et al., 2002; Mei and Kohlstedt, 2000a,b; Rutter and Neumann, 1995; van der Molen and Paterson, 1979). The dependence of the solid-state viscosity on the melt fraction is parameterized with the help of simple exponential function:

$$\eta = \eta_s \exp(-\alpha_\eta \phi) \quad [18]$$

where η_s is the viscosity of melt-free rock and α_η is a constant that depends on the creep mechanism. Mei et al. (2002) gave $\alpha_\eta = 26$ for diffusion creep and $\alpha_\eta = 31$ for dislocation creep.

9.04.5 Convection in the Magma Ocean

9.04.5.1 Convective Heat Flux

During the early stages of crystallization of the magma ocean, the viscosity is small and convection is extremely turbulent. The convective heat flux is usually calculated as

$$F_{soft} = 0.089 \frac{k(T_m - T_s)}{L} Ra^{1/3} \quad [19]$$

where

$$Ra = \frac{\alpha g (T_m - T_s) L^3}{\kappa \nu} \quad [20]$$

is the Rayleigh number, T_m is the potential temperature of the magma ocean, T_s is the surface temperature, k is the coefficient of thermal conductivity, $\kappa = k/\rho c_p$ is the coefficient of thermal diffusivity, and $\nu = \eta/\rho$ is the kinematic viscosity (Kraichnan, 1962; Siggia, 1994).

However, at very high Rayleigh numbers such as those in the magma ocean, convection changes to a regime sometimes called hard turbulence (Castaing et al., 1989; Grossmann and Lohse, 1992; Shraiman and Siggia, 1990; Siggia, 1994). By contrast, the ordinary turbulence is called soft turbulence. One of the important features of hard-turbulent convection is the existence of a large-scale circulation. This coherent motion within the highly turbulent fluid is an example of self-organization in complex systems (e.g., Nicolis and Prigogine, 1977), that is, systems that have many degrees of freedom interacting with each other. Turbulence is caused by numerous plumes originating from the upper and lower boundaries of the convective layer. The coherent circulation of the fluid emerges from random actions of these plumes. In the magma ocean, this mainly includes cold plumes originating from the surface but may also include hot plumes originating from the core–mantle boundary.

Several scaling laws have been proposed for the hard turbulence regime (Kadanoff, 2001; Siggia, 1994). Shraiman and Siggia (1990) obtained the following equation:

$$F_{hard} = 0.22 \frac{k(T_m - T_s)}{L} Ra^{2/7} Pr^{-1/7} \lambda^{-3/7} \quad [21]$$

where $Pr = \nu/\kappa$ is the Prandtl number and λ is the aspect ratio for the mean flow.

Another effect to consider is the rotation of the Earth. Although the rotation of the Earth does not affect subsolidus mantle dynamics (Coriolis forces are negligible compared to viscous forces), the dynamics of low-viscosity magma ocean may be affected by rotation. How large is the effect of rotation on the heat flux? At low Rayleigh numbers (soft turbulence), the heat flux depends on the rotation as follows:

$$F \sim \frac{k(T_m - T_s)}{L} Ra^3 Ta^{-2} \quad [22]$$

where

$$Ta = \frac{4\Omega^2 L^4}{\nu^2} \quad [23]$$

is the Taylor number (Boubnov and Golitsyn, 1986, 1990; Canuto and Dubovikov, 1998).

At high Rayleigh numbers, the effect of rotation becomes negligible and the heat flux is the same as in the absence of rotation. The critical Rayleigh number for the transition to the no-rotation regime is approximately the one at which the two scaling laws (with and without rotation) give the same heat flux. In the soft turbulence regime, the requirement that the heat flux [19] is the same as [22] gives the Rayleigh number above which rotation does not affect the heat flux (see also Canuto and Dubovikov, 1998):

$$Ra_* \sim Ta^{3/4} \quad [24]$$

For the magma ocean, $Ta \sim 10^{25}$. This gives $Ra_* \sim 10^{19}$, which is much smaller than the typical values $Ra \sim 10^{28}$–10^{29}. Although these estimates are for soft turbulence, the difference between soft turbulence and hard turbulence is relatively small. Thus, it is reasonable to assume that rotation does not have any significant effect on the heat flux in the hard turbulence regime.

Application of the hard turbulence regime to magma oceans requires substantial extrapolation: Laboratory experiments have only been performed on helium ($Pr \sim 1$) to about $Ra \sim 10^{17}$, while in the magma ocean, $Ra \sim 10^{28}$–10^{29} and $Pr \sim 10^2$–10^3. At very high Rayleigh numbers, convection was expected to enter a new regime of turbulent convection (Kraichnan, 1962; Siggia, 1994). So far, experiments did not show any evidence of such an 'ultrahard' regime (Glazier, 1999; Niemela et al., 2000). Thus, hard turbulence is probably applicable to the extreme conditions of magma oceans.

The spherical geometry of the magma ocean is different from the geometries in laboratory experiments. However, like in other convection problems, the changes in the scaling laws due to spherical geometry are expected to be minor. A major uncertainty associated with spherical geometry is probably the aspect ratio λ of the mean flow. The simplest assumption is that $\lambda \sim 1$, that is, the horizontal scale of the mean flow is of the order of the depth of the magma ocean. This parameter can be effected by rotation.

Temperature-dependent viscosity does not seem to play a significant role in controlling the heat flux. When the potential temperature is close to liquidus, the temperature contrast in the thermal boundary layer is 200–600 K depending on the scaling law. According to Liebske et al. (2005b), the corresponding viscosity contrast is at most one order of magnitude. This is too small to have a significant effect on the heat transport (Solomatov, 1995a).

Does radiative heat transport play a role in the thermal boundary layer near the surface? The thickness $\delta = k(T_m - T_s)/F$ of the thermal boundary layer is of the order of 1 cm. The free path of infrared photons in silicates is smaller, of the order of 1 mm (Clark, 1957; Shankland et al., 1979). This means that the thermal boundary layer is not thin enough to be transparent to infrared radiation. Also, the thermal conductivity of magma does not seem to be significantly affected by the radiative heat transport. The data collected by Murase and McBirney (1973) suggest that for solid lherzolite, the thermal conductivity is not very different from that at low temperatures: $k \approx 4\,\mathrm{W\,m^{-1}\,K^{-1}}$ around 1500 °C.

The heat flux depends on the surface temperature. Since the heat flux from the magma ocean is much higher than the incoming solar radiation, the surface temperature is established not by the radiative equilibrium between the incoming radiation and outgoing radiation but by the equilibrium between the heat flux transported by convection in the magma ocean to the surface and the heat flux radiated from the surface of the magma ocean. The latter depends on the type of the atmosphere covering the magma ocean (Abe and Matsui, 1986; Hayashi et al., 1979; Matsui and Abe, 1986; Nakazawa et al., 1985; Zahnle et al., 1988). In the early stages of crystallization, the surface temperature is very high, more than 2000 K. In this case, the atmosphere is a 'silicate' one (Hayashi et al., 1979; Nakazawa et al., 1985; Thompson and Stevenson, 1988). The heat flux can be written as

$$F = \sigma_{SB} T_e^4 \quad [25]$$

where T_e is the effective temperature (the temperature that corresponds to a blackbody emitting the heat flux F) and $\sigma_{SB} = 5.67 \times 10^{-8}\,\mathrm{J\,m^{-2}\,K^{-4}}$ is the Stefan–Boltzmann constant. The magnitude of T_e depends on the mass of the silicate atmosphere. It can be smaller than the surface temperature T_s by several hundred kelvins (Thompson and Stevenson, 1988). Fortunately, the dependence on the mass of the atmosphere is weak. The simplest assumption one can make without considering the heat transfer in the atmosphere is that $T_e \approx T_s$, that is, magma ocean radiates like a blackbody with temperature T_s. With this assumption, the surface heat flux can be overestimated by a factor of $(T_s/T_e)^4$. For a moderately opaque atmosphere with $T_e \approx 1500\,\mathrm{K}$ and $T_s \approx 2000\,\mathrm{K}$, $(T_s/T_e)^4 \sim 3$.

Figure 4 shows the heat flux and the surface temperature as functions of the potential temperature of the magma ocean during the initial period of crystallization. The scaling law for

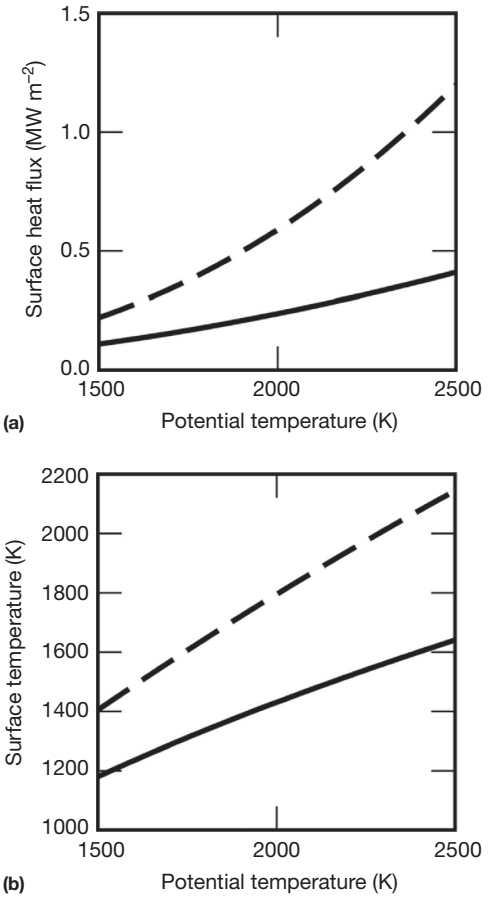

Figure 4 (a) The surface heat flux and (b) the surface temperature are shown as functions of the potential temperature calculated using scaling laws for soft turbulence convection (solid line) and hard turbulence convection (dashed line). The viscosity is $\eta_l = 0.1$ Pa s. The uncertainties associated with the viscosity are smaller than those associated with the scaling law.

hard-turbulent convection predicts that the heat flux is close to $10^6\,\mathrm{W\,m^{-2}}$. The formula for soft-turbulent convection gives lower values of the heat flux, by a factor of ~ 3. It might be worth emphasizing that these are only rough estimates. Also, a more realistic model would need to consider a coupled evolution of the atmosphere and magma ocean, which is a significantly more complex problem (Abe, 1997; Elkins-Tanton, 2011; Marcq, 2012) especially given its highly stochastic nature (Abe, 2011).

9.04.5.2 Convective Velocities

In the soft turbulence regime, the convective velocities can be estimated in terms of the mixing length l as (Kraichnan, 1962; Priestly, 1959)

$$u_0 \approx 0.6\left(\frac{\alpha g l F}{\rho c_\mathrm{p}}\right)^{1/3} \quad [26]$$

where F is the surface heat flux. The coefficient is constrained by laboratory experiments (Deardorff, 1970; Willis and Deardorff, 1974) and atmospheric measurements (Caughey and Palmer, 1979). The simplest assumption is that the mixing length is approximately equal to the depth of the magma ocean $l \sim L$ (if the magma ocean has partially crystallized beyond the rheological transition, then l should be the thickness of the remaining low-viscosity region). For $F \approx 10^6\,\mathrm{W\,m^{-2}}$ (**Figure 4**) and other parameters from **Table 1**, eqn [26] gives $u_0 \sim 4\ \mathrm{m\ s^{-1}}$ (note that the velocity is slightly larger in two-phase regions where α and c_p need to be replaced by eqns [3] and [4]).

The ratio F/ρ is almost the same for the magma ocean and the atmosphere. This explains why the previous estimate is very similar to the observed velocities in the convective boundary layer in the atmosphere (Caughey and Palmer, 1979).

The equations suggested by Shraiman and Siggia (1990) can be rewritten in the form similar to eqn [26]:

$$u_0 \approx a_u\left(\frac{\alpha g l F}{\rho c_\mathrm{p}}\right)^{1/3} \quad [27]$$

where the coefficient $a_u \approx 0.086 x^*$ and x^* is related to u_0 through the following equation:

$$x^* = 2.5 \ln\left[\frac{\rho u_0 l}{\eta}\frac{1}{x^*}\right] + 6 \quad [28]$$

The solution to the earlier transcendental equations gives $a_u \approx 5.9$, which varies weakly with $\rho u_0 l/\eta$. In the hard turbulence regime, the velocity increases by a factor of 10. This brings the estimate of the convective velocity in the magma ocean up to $40\ \mathrm{m\,s^{-1}}$. The effect of the Earth's rotation can be estimated in the same way as it was done for soft turbulence: replacing the thickness of the convective layer by a reduced length scale

$$l \sim \frac{u_0}{\Omega} \quad [29]$$

imposed by rotation explains rather well the experimentally observed reduction in the convective velocity (Boubnov and Golitsyn, 1986, 1990; Chen et al., 1989; Fernando et al., 1991; Golitsyn, 1980, 1981; Hopfinger, 1989; Hopfinger et al., 1982; Solomatov and Stevenson, 1993a).

Assuming that this length scale works for hard turbulence, Solomatov (2000) obtained

$$u_0 \approx 14\left(\frac{\alpha g F}{\rho c_\mathrm{p} \Omega}\right)^{1/2} \quad [30]$$

This gives velocities around $16\ \mathrm{m\,s^{-1}}$ with the uncertainty of a factor of 3. The value of $10\ \mathrm{m\,s^{-1}}$ can be assumed for the magma ocean (**Table 1**).

9.04.6 Fractional Versus Equilibrium Crystallization

9.04.6.1 How Are Crystals Suspended by Convection?

Early studies of convective suspensions used several approaches. Some looked at the trajectories of particles in steady flows and assumed that the particles whose trajectories are closed can be suspended indefinitely (Marsh and Maxey, 1985; Rudman, 1992; Weinstein et al., 1988). This approach cannot work for turbulent flows where closed trajectories do not exist.

Others used a phenomenological description of the balance between the downward flux of particles due to settling and the upward flux due to convection (Bartlett, 1969; Huppert and Sparks, 1980). This approach predicted that crystals stay in suspension if the settling velocity is smaller than the convective velocity.

However, this approach did not consider the fact that the convective velocities decrease near the bottom. The first systematic laboratory experiments on convective suspensions by Martin and Nokes (1988, 1989) showed that even when the settling velocity is much smaller than the convective velocity, the particles eventually settle down and they do so nearly as fast as in the absence of convection. They argued that because the convective velocity at the lower boundary vanishes, the particles cannot be reentrained and remain at the boundary. Yet, in one experiment, the amount of suspended particles remained constant after some partial initial sedimentation.

Tonks and Melosh (1990) addressed the problem of suspension in convective systems using the analogy with the entrainment of particles in shear flows. They argued that turbulence is the key factor for suspension for both shear flows and convection. According to their arguments, turbulence was not strong enough in Martin and Nokes' (1988, 1989) experiments. In particular, they argued that sedimentation in convective systems does not occur if the settling velocity is smaller than the effective friction velocity associated with turbulent fluctuations. However, Solomatov and Stevenson (1993a) pointed out that the Reynolds number in the only experiment where Martin and Nokes reported suspension was about 0.03, which is below the critical value for the transition to turbulence by two orders of magnitude. Thus, it remained unclear how particles are reentrained from the bottom.

Solomatov et al. (1993) investigated the mechanisms of entrainment experimentally using polystyrene spheres in an aqueous $CaCl_2$ solution. They showed that for either laminar or turbulent convection, the particles are moved at the bottom by the stresses generated by thermal plumes. These stresses are much larger than the stresses generated by turbulence. They also showed that the particles are not reentrained right away

but they are piled together in 'dunes.' If the flow is strong enough, it picks up the particles at the crests of the dunes and reentrains them back into the interior region of the convective layer. The critical condition for reentrainment is

$$\frac{\tau_T}{\Delta\rho g d} \sim 0.1 \quad [31]$$

where

$$\tau_T = \left(\frac{\eta_l \alpha g F}{c_p}\right)^{1/2} \quad [32]$$

is the convection stress scale and d is the diameter of the particles.

Application of these criteria to magma oceans is still not straightforward because the conditions in magma oceans are quite different from the laboratory experiments. Although the stress [32] dominates at low Rayleigh numbers, at high Rayleigh numbers, the situation can reverse. In fact, in the hard turbulence regime, the stresses associated with turbulence are larger than [32] (Shraiman and Siggia, 1990). The former are

$$\tau^* = \rho u^{*2} \quad [33]$$

where $u^* = u_0/x^*$ (eqn [28]). With typical values of $x^* \sim 60$ and $u_0 \sim 10\ \mathrm{m\,s^{-1}}$, one gets $\tau^* \sim 50\ \mathrm{Pa}$. Assuming that eqn [31] can be applied to the hard turbulence regime, that is,

$$\frac{\tau^*}{\Delta\rho g d} \sim 0.1 \quad [34]$$

one can get that crystals up to several centimeters in diameter can be suspended in magma oceans. The criterion [31] gives much smaller critical crystal size, by almost two orders of magnitude.

Perhaps a more important factor is that unlike non-interacting particles in the laboratory experiments, crystals can form solid bonds as observed in experiments on magmas (e.g., Lejeune and Richet, 1995). Formation and growth of solid bonds are a well-studied phenomenon in metallurgy, which plays a key role in liquid phase sintering (e.g., German, 1985). The bonds between crystals and the underlying bed can easily prevent reentrainment.

9.04.6.2 Energetics of Convective Suspensions

Even though reentrainment of crystals from the bottom of the convective layer is the key process that keeps particles suspended in laboratory experiments, this is not the most important factor that controls sedimentation in magma oceans. The crucial factor for magma oceans is that the presence of crystals can suppress convection as a result of viscous heating and density stratification associated with crystal settling (Solomatov and Stevenson, 1993a).

The total amount of energy released per unit time due to crystal settling is

$$\Phi = u_s g \phi \Delta\rho V \quad [35]$$

where u_s is the settling velocity and V is the volume of the magma ocean. Thus, convection has to do work to suspend crystals.

The total amount of energy per unit time, which is available for mechanical work, is

$$W \approx \frac{\alpha g L}{c_p} FA \approx FA \quad [36]$$

where A is the surface area of the Earth and $\alpha g L/c_p \sim 1$. Most of this work is spent to overcome viscous friction associated with convection, that is, just to keep convection going.

Experiments show that only a small fraction $\varepsilon \sim 0.1$–1% of W is available for reentrainment (Solomatov et al., 1993) If reentrainment is possible, the equilibrium volume fraction of crystals is determined by the condition that

$$\Phi = \varepsilon W \quad [37]$$

When $\Phi > \varepsilon W$, the sedimentation rate exceeds the reentrainment rate and vice versa.

When viscous dissipation due to sedimentation exceeds the available mechanical power, that is,

$$\Phi > W \quad [38]$$

convection is suppressed and suspension ceases to exist (Solomatov and Stevenson, 1993a). Although this theoretical prediction has not been tested experimentally, Solomatov and Stevenson (1993a) showed that this condition approximately coincides with the condition that the turbulence collapses due to density stratification caused by crystal settling (Solomatov and Stevenson, 1993a). The latter problem is analogous to the problem of turbulence in stratified fluids and has been well studied in laboratory experiments (Hopfinger, 1987).

When viscous dissipation exceeds the total heat loss rate from the magma ocean, that is,

$$\Phi > FA \quad [39]$$

then cooling can continue only after fractionation of some amount of crystals reduces Φ to the level where $\Phi < FA$.

9.04.6.3 Conditions for Fractional Crystallization

Fractional crystallization is expected to happen when the condition [39] is satisfied (cooling is impossible without sedimentation) and even when a less severe condition [38] is satisfied (convection is suppressed) although for deep magma oceans, these two conditions almost coincide. In either case, crystal–melt segregation occurs independently of whether or not there is any reentrainment of crystals at the bottom of the magma ocean.

To estimate the crystal size at which this happens, we need the equation for the settling velocity

$$u_s = f_\phi \frac{\Delta\rho g d^2}{18\eta_l} \quad [40]$$

where f_ϕ is a hindered settling function such that $f_\phi = 1$ at $\phi = 0$ (Davis and Acrivos, 1985). If the crystal fraction in the magma ocean varies from 0 to the maximum packing fraction $\phi_m = 0.6$, then the average crystal fraction is about $\phi \sim 30\%$ at which $f_\phi \sim 0.15$ (Davis and Acrivos, 1985).

The critical crystal size above which fractional crystallization occurs is then found from eqn [38]:

$$d_f = \left(\frac{18\alpha\eta_l FAL}{f_\phi g c_p \Delta\rho^2 \phi V}\right)^{1/2} \quad [41]$$

or

$$d_f \approx 10^{-3}\left(\frac{\eta_l}{0.1\,\text{Pa s}}\right)^{1/2}\left(\frac{F}{10^6\,\text{W m}^{-2}}\right)^{1/2}\text{m} \quad [42]$$

9.04.6.4 Conditions for Equilibrium Crystallization

A simple condition for the magma ocean to crystallize without any substantial chemical differentiation is one that requires that the sedimentation time is much smaller than the crystallization time (Solomatov, 2000).

The crystallization time is

$$t_c \approx \frac{(\Delta H\phi + c_p\Delta T)M}{FA} \approx 400\,\text{years} \quad [43]$$

where $\Delta T \sim 1000$ K is the average temperature drop upon crystallization of the magma ocean up to the crystal fraction $\phi \sim 60\%$ and M is the mass of the magma ocean.

The sedimentation time even in the presence of turbulent convection is (Martin and Nokes, 1988)

$$t_s \approx \frac{L}{u_s} \quad [44]$$

Crystallization is faster than sedimentation, that is, $t_c < t_s$, provided the crystal size is smaller than

$$d_e = \left(\frac{18L\eta_l}{f_\phi g\Delta\rho t_c}\right)^{1/2} \quad [45]$$

or

$$d_e \approx 10^{-3}\left(\frac{\eta_l}{0.1\,\text{Pa s}}\right)^{1/2}\left(\frac{F}{10^6\,\text{W m}^{-2}}\right)^{1/2}\text{m} \quad [46]$$

The difference between d_f and d_e is negligible compared to the uncertainties in the crystal size. Therefore, the critical crystal size that separates equilibrium and fractional crystallization is

$$d_{crit} \approx 10^{-3}\left(\frac{\eta_l}{0.1\,\text{Pa s}}\right)^{1/2}\left(\frac{F}{10^6\,\text{W m}^{-2}}\right)^{1/2}\text{m} \quad [47]$$

The fact that these two estimates are very close to each other is not surprising – their ratio scales approximately as

$$\frac{d_e}{d_f} \sim \left(\frac{\Delta\rho/\rho c_p}{\alpha T\Delta S}\right)^{1/2} \quad [48]$$

where we used $M \sim \rho AL$ and $\Delta H\phi + c_p\Delta T \sim \Delta H\phi \sim T\Delta S\phi$.

The entropy change upon melting ΔS is of the order of several k_B per atom (Stishov, 1988), while $c_p = 3k_B$ per atom. Therefore, $\Delta S \sim c_p$. Also, $\Delta\rho/\rho \sim \alpha T \sim 0.1$. Thus, $d_e/d_f \sim 1$.

9.04.7 Crystal Size in the Magma Ocean

The estimate of the critical crystal size $\sim$1 mm separating equilibrium and fractional crystallization is significantly smaller than the early estimates, which predicted that the critical crystal size is of the order of tens of meters (Miller et al., 1991a,b; Tonks and Melosh, 1990). If the critical crystal size were indeed this big, no physical mechanism could allow the crystals to reach this size during the lifetime of the magma ocean. The new estimate is in the range of typical crystal sizes observed in magmas (e.g., Cashman and Marsh, 1988), thus bringing up the question of whether the crystal size in the magma ocean was larger or smaller than $\sim$1 mm.

9.04.7.1 What Processes Control the Crystal Size in the Magma Ocean?

In thermodynamic equilibrium, the crystal diameter d is related to the crystal fraction ϕ and the number of crystals N per unit volume as (assuming spherical shape)

$$d = \left(\frac{6\phi}{\pi N}\right)^{1/3} \quad [49]$$

The number of crystals is controlled by nucleation in the descending flow. When crystal-free magma reaches the pressure where the temperature of the convecting magma ocean (adiabat) drops below the liquidus, crystals nucleate and grow until the equilibrium crystal fraction is reached.

If the number of crystals does not change with time, then the crystals grow simply because the equilibrium crystal fraction ϕ changes with depth along the adiabat – increases on the way down and decreases on the way up. However, dissolution of smaller crystals and growth of larger crystals decrease the number of crystals per unit volume and, thus, increase the average crystal size according to eqn [49]. This process is called Ostwald ripening.

9.04.7.2 Nucleation

When the temperature in the downwelling convective flow drops below the liquidus, crystals form via nucleation and growth mechanism (Figures 5 and 6). During nucleation, tiny crystals (tens of atoms in diameter, depending on the supercooling) precipitate from the supercooled melt. The

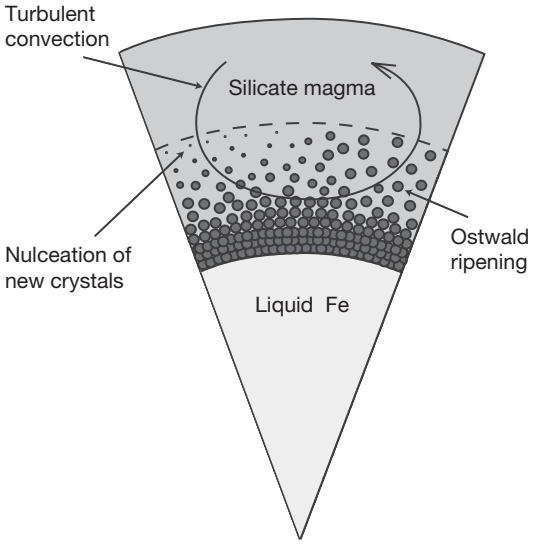

Figure 5 Magma ocean in the early stages of crystallization. Nucleation occurs in the downgoing convective flow when it enters the two-phase region. Crystals continue to grow because of Ostwald ripening – larger crystals grow at the expense of smaller ones. The crystals that have resided longer in the two-phase region are schematically shown bigger.

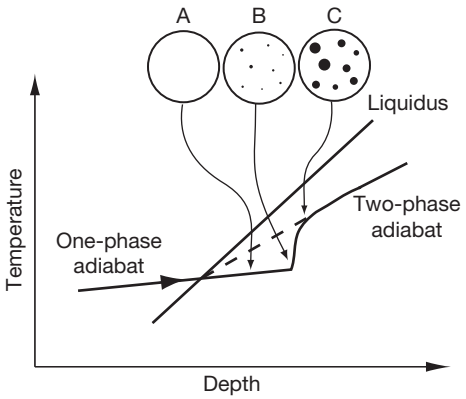

Figure 6 Evolution of a fluid parcel (large circle) in the downwelling flow. When the temperature of a fluid parcel drops below the liquidus, the temperature of the parcel initially follows a metastable one-phase adiabat (solid line) rather than the two-phase adiabat (dashed line), without any crystallization (stage A – pure liquid). When the supercooling reaches the nucleation barrier, an avalanche-like nucleation produces tiny crystals (stage B – liquid with nuclei). The subsequent crystal growth brings the temperature of the fluid up to the equilibrium two-phase adiabat (stage C – nearly equilibrium liquid–crystal mixture).

nucleation rate (the number of nuclei produced per unit volume per unit time) is an extremely sensitive function of the supercooling $\Delta T = T_{\mathrm{liq}} - T$ – the difference between the equilibrium value of the liquidus and the actual temperature of the fluid. It can approximately be described as

$$J(\Delta T) = a \exp\left(-\frac{B}{\Delta T^2}\right) \qquad [50]$$

$$B = \frac{16\pi\sigma_{\mathrm{app}}^3 T_0^2}{3k_{\mathrm{B}} T \rho^2 \Delta H^2} \qquad [51]$$

where a is a constant, T_0 is the melting temperature of the crystallizing phase, and σ_{app} is the apparent surface energy. Once a crystal has nucleated, it grows at a rate that can be controlled by either interface kinetics or diffusion. In the former case, the bottleneck in crystal growth is the attachment of atoms to the crystal (e.g., in some cases, the atom needs to find an imperfection on the crystal surface to be able to attach to it), while in the latter case, the attachment is relatively easy and the bottleneck is the long-range transport of atoms in the melt surrounding the growing crystal.

Although nucleation and crystal growth in the magma ocean might seem to be very difficult to constrain, fortunately, this process is mathematically very similar to bulk crystallization of continuously cooling liquids in laboratory conditions (Cashman, 1993; Flemings et al., 1976; Grove, 1990; Grove and Walker, 1977; Ichikawa et al., 1985; Lofgren et al., 1974; Smith et al., 1991; Walker et al., 1978). In both cases, the controlling parameter is the cooling rate $\dot{T}$. The only difference is that the effective cooling rate of an adiabatically descending fluid parcel is the rate of change of the difference between the liquidus temperature T_{liq} and the adiabatic temperature T_{ad}:

$$\dot{T} = u_0 \left(\frac{\mathrm{d}T_{\mathrm{liq}}}{\mathrm{d}z} - \frac{\mathrm{d}T_{\mathrm{ad}}}{\mathrm{d}z}\right) \qquad [52]$$

where $\mathrm{d}T_{\mathrm{liq}}/\mathrm{d}z$ is the liquidus gradient and $\mathrm{d}T_{\mathrm{ad}}/\mathrm{d}z$ is the adiabatic gradient.

Solomatov and Stevenson (1993c) solved the problem of nucleation in continuously cooling multicomponent liquids for interface kinetics controlled growth. Their solution is somewhat similar to the one obtained by Raizer (1960) (see also Zel'dovich and Raizer, 2002) for condensation in an adiabatically expanding cloud of vapor except that it uses a more general mathematical method developed by Buyevich and Mansurov (1991). Solomatov (1995b) solved this problem for the case when crystal growth is controlled by diffusion rather than interface kinetics and showed that this solution is more consistent with various experimental data on silicates and alloys.

According to Solomatov (1995b), nucleation in continuously cooling liquids operates during a very short period of time (an avalanche-like event). The abrupt start of nucleation is due to the fact that the liquid needs to reach a critical supersaturation (the nucleation barrier). The short duration and abrupt cessation of the nucleation are due to the fact that the precipitated crystals quickly change the composition of the fluid, which reduces the supersaturation below the nucleation barrier. Although the duration of nucleation is short, this is the key process that determines the number of crystals nucleated per unit volume, and thus, the size of these crystals after the system reaches an equilibrium.

The number of nuclei produced per unit volume during the nucleation period is calculated as follows:

$$N = 0.2 \frac{\zeta^{3/2} \dot{T}^{3/2} \theta^{3/2}}{B \left|\mathrm{d}T_{\mathrm{liq}}/\mathrm{d}\phi\right| D^{3/2}} \qquad [53]$$

where D is the diffusion coefficient and $\zeta = \Delta T/\Delta C$ determines the relationship between the supercooling ΔT and the supersaturation ΔC. It is of the order of the difference between liquidus and solidus temperatures, $\zeta \sim T_{\mathrm{liq}} - T_{\mathrm{sol}}$.

The parameter θ in eqn [53] is nearly constant (~30). It can be found from the transcendental equation

$$\theta = \ln\left[\frac{6.05\left|\mathrm{d}T_{\mathrm{liq}}/\mathrm{d}\phi\right| a B^{3/2} D^{3/2}}{\zeta^{3/2} \dot{T}^{5/2} \theta^3}\right] \qquad [54]$$

From eqns [49] and [53] with $\phi \sim 60\%$, we estimate

$$d_{\mathrm{nucl}} \approx 10^{-3} \left(\frac{\sigma_{\mathrm{app}}}{0.02\,\mathrm{J\,m^{-2}}}\right) \left(\frac{D}{10^{-9}\,\mathrm{m^2\,s^{-1}}}\right)^{1/2} \left(\frac{u_0}{10\,\mathrm{m\,s^{-1}}}\right)^{-1/2} \mathrm{m} \qquad [55]$$

This relationship can be interpreted as follows. The velocity controls the cooling rate of fluid parcels: the faster the cooling rate, the further the system is driven into the metastable state, the higher the nucleation rate and the more crystals are nucleated. This corresponds to the well-known fact that faster cooling produces smaller crystals. The diffusion coefficient controls the crystal size somewhat indirectly: during the nucleation and growth stage, the thermodynamic equilibrium is achieved via both the nucleation of new crystals and the growth of already nucleated crystals. The larger the diffusion coefficient, the more this balance is shifted toward growth and the fewer crystals are nucleated. The surface energy controls nucleation: the larger the surface energy, the more difficult it is to nucleate crystals and the fewer crystals are produced.

Note that the apparent cooling rates $\dot{T}$ in the magma ocean are not that much different from those in the laboratory

conditions (Figure 7). This means that there is no extrapolation in this parameter. The parameter that can significantly affect the estimate of the crystal size is the apparent surface energy, σ_{app}. It was argued that it is not the normal surface energy but rather an apparent one for nucleation (Dowty, 1980; Solomatov, 1995b). The value of 0.02 $J\,m^{-2}$ (Table 1) is based on the analogy with other cases that suggest that it is almost one order of magnitude smaller compared to the usual one. Higher values of σ_{app} in the magma ocean cannot be excluded. This means that it can increase the crystal size by as much as one order of magnitude.

It is also worth noting that because of a large value of the logarithm in eqn [54], the value of θ and thus, the crystal size, is insensitive to the uncertainties in the parameters under the logarithm. In particular, the most uncertain parameter is the prefactor a (the uncertainties can be as large as 10 orders of magnitude). However, this uncertainty effects the results only by a factor of 2 or so.

9.04.7.3 Ostwald Ripening

For diffusion-controlled Ostwald ripening, crystal size is calculated as follows (Lifshitz and Slyozov, 1961; Voorhees, 1992):

$$d_{ost}^3 - d_{nucl}^3 = \frac{32}{9} b_\phi \alpha_0 D t_{ost} \qquad [56]$$

where d_{nucl} is the initial crystal size after nucleation, $\alpha_0 = 2\sigma c_\infty v_m / RT$, σ is the surface energy, c_∞ is the equilibrium concentration of the crystallizing mineral in the melt, v_m is the molar volume of the crystallizing mineral, t_{ost} is the time available for Ostwald ripening, and b_ϕ is a function of ϕ such that $b_\phi = 1$ in the limit $\phi \ll 1$. The time available for Ostwald ripening is roughly the characteristic residence time in the two-phase region, that is, $t_{ost} \sim H/u_0$. Neglecting the initial crystal size d_{nucl}, we obtain that

$$d_{ost} \approx 10^{-3} \left(\frac{D}{10^{-9}\,m^2\,s^{-1}}\right)^{1/3} \left(\frac{u_0}{10\,m\,s^{-1}}\right)^{-1/3} m \qquad [57]$$

This is similar to estimate [55]. Thus, Ostwald ripening does not increase the crystal size substantially.

The previous estimates show that the crystal size during the early crystallization of the magma ocean is very close to the critical crystal size separating fractional and equilibrium crystallization of the magma ocean (Figure 8), which is about 1 mm. This means that both equilibrium and fractional crystallization (up to 60% crystal fraction) are equally acceptable within the uncertainties of the physical parameters.

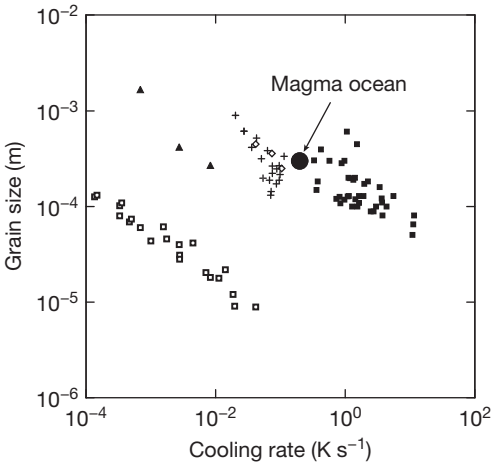

Figure 7 Crystal size versus cooling rate for five crystallizing phases (from Solomatov, 1995b): Sn (Sn–Pb system, solid boxes), Al (Al–Cu, pluses), Si (Al–Si, diamonds), diopside (diopside–plagioclase, solid triangles), and plagioclase (diopside–plagioclase, open boxes). The data are from Lofgren et al. (1974), Flemings et al. (1976), Grove and Walker (1977), Walker et al. (1978), Ichikawa et al. (1985), Grove (1990), Smith et al. (1991), and Cashman (1993). The data approximately follow the theoretical 1/2 slope. The location of the magma ocean is shown.

9.04.8 Crystallization Beyond the Rheological Transition

As was mentioned earlier, at the crystal fraction around $\phi_m \sim 60\%$, crystal–melt mixture undergoes a rheological transition to a solid-like behavior, and the deformation is controlled by the solid-state creep of crystals. Solomatov and Stevenson (1993b) and Solomatov (2000) showed that rapid cooling and crystallization may continue even at $\phi > \phi_m$.

This can be explained as follows. When the viscosity of magma abruptly increases from liquid-like viscosity to the solid-like viscosity around $\phi \sim \phi_m$, convection stops at the bottom of the magma ocean or somewhere near it – the hot core may keep the base of the mantle molten even after crystallization of the magma ocean. A nonconvecting layer with the crystal fraction $\phi \sim \phi_m$ starts growing from the bottom of the magma ocean (Figure 9). If solid-state convection does not start, then in about 400 years, eqn [43], the temperature in the entire magma ocean would approximately follow the curve $\phi \sim \phi_m = \text{const}$. However, the temperature gradient of the magma ocean, which is partially crystallized to $\phi \sim \phi_m$, is

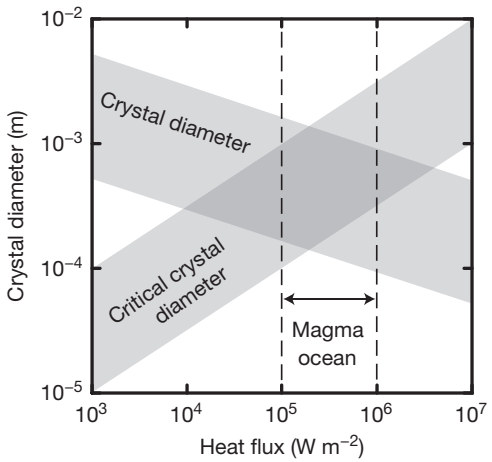

Figure 8 The crystal size during the early stages of crystallization of the magma ocean (assuming that it is controlled by nucleation in the downwelling flow) and the critical crystal size for suspension are shown as functions of the heat flux. The width of the curves (gray bands) represents the uncertainty range of one order of magnitude.

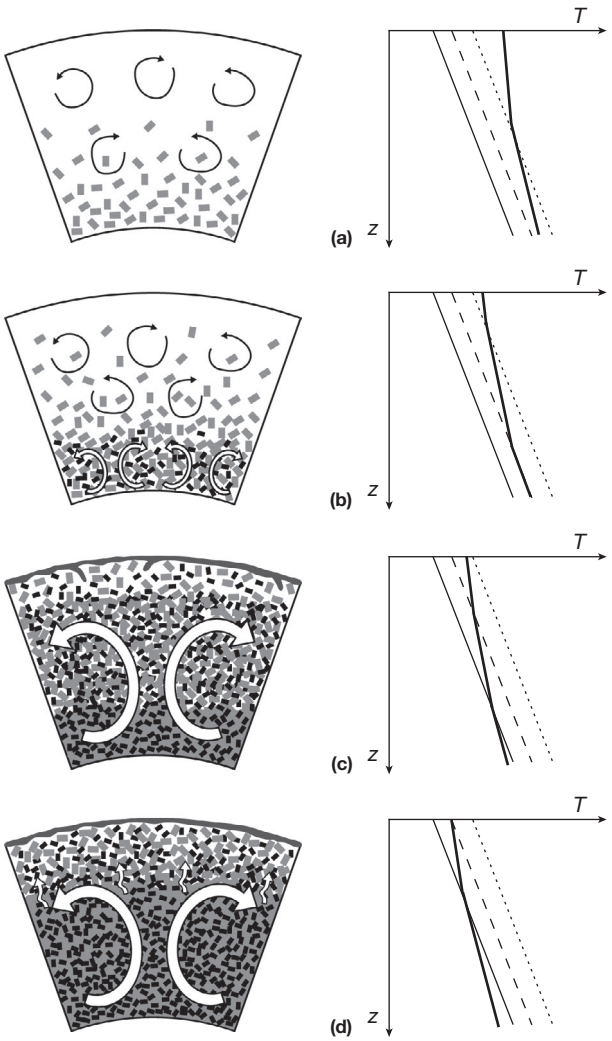

Figure 9 Crystallization of the magma ocean: (a) The lower part of the magma ocean is below liquidus (dotted line), convection is controlled by melt viscosity, and the temperature (heavy solid line) is adiabatic; (b) high-viscosity, gravitationally unstable region with the maximum packing crystal fraction forms near the bottom of the magma ocean ($\phi = \phi_m$ curve is shown with a dashed line); (c) cooling beyond $\phi = \phi_m$ proceeds via solid-state convection, which is still fast at this stage. The temperature in the high-viscosity region below solidus (solid line) can be superadiabatic; (d) $\phi > \phi_m$ everywhere and the rate of cooling and crystallization of the remaining melt are controlled by solid-state convection and melt percolation. The gray and black crystals schematically illustrate different mineral phases.

roughly parallel to solidus and thus is steeper than the adiabat. Since the adiabat is the temperature profile of a neutrally stable fluid, a superadiabatic temperature profile would make the mantle gravitationally unstable.

The instability is so fast that one can ignore thermal diffusion and treat it like a Rayleigh–Taylor instability. The driving effective density contrast is of the order of

$$\Delta\rho_{RT} \approx \frac{1}{2}\alpha\rho L\left(\frac{dT_{sol}}{dz} - \frac{dT_{ad}}{dz}\right) \approx 100\,\mathrm{kg\,m^{-3}} \qquad [58]$$

for the whole mantle ($L \approx 3 \times 10^6$ m).

The timescale for the overturn can then be estimated as (Turcotte and Schubert, 2002)

$$t_{RT} \approx 26\frac{\eta_s}{\Delta\rho_{RT} g L} \qquad [59]$$

where η_s is the viscosity of the solid mantle and g is the gravity.

The viscosity η_s of the lower mantle is poorly constrained. The present-day lower mantle viscosity is around 10^{22} Pa s (e.g., King, 1995). The temperature of the mantle is much below solidus, by ~1000–1500 K at the base of the mantle (Boehler, 1996, 2000; Zerr et al., 1998). Thus, the viscosity near the solidus must be substantially lower than 10^{22} Pa s. Based on experimental and theoretical constraints on the lower mantle viscosity (Béjina et al., 2003; Ita and Cohen, 1998; Karato and Li, 1992; Li et al., 1996; Wright and Price, 1993; Yamazaki and Karato, 2001; Yamazaki et al., 2000), we can assume that the viscosity near the solidus is about 10^{18} Pa s for the grain size of 10^{-3} m.

The presence of melt reduces the viscosity further. Equation [18] suggests that the viscosity is ~10^4–10^5 times smaller at $\phi \sim \phi_m$ and one order of magnitude smaller when only 10% melt remains in the mantle. These estimates are very approximate because eqn [18] is a phenomenological equation whose underlying physical mechanisms are poorly understood and thus the errors due to extrapolation to the magma ocean conditions are unknown. Nevertheless, eqns [18] and [59] predict that for a near-solidus mantle, the overturn is of the order of 100 years, and for $\phi \sim \phi_m$, it can be as short as a few days.

Thus, the instability starts developing soon after the maximum packing fraction is reached at the bottom of the magma ocean and takes the form of solid-state convection, which is the primary mechanism of cooling and crystallization in the range $\phi_m < \phi < 1$. A complete solidification front would follow the rheological front toward the surface (**Figure 9**). When the adiabatic temperature in the solidified regions becomes so low that the viscosity exceeds about 10^{19} Pa s, then Rayleigh–Taylor will be unable to catch up with the solidification front. It is likely that the temperatures in the high-viscosity regions will be superadiabatic. In this case, a substantial superadiabatic temperature gradient can be created upon crystallization of the magma ocean. The instability would continue after crystallization of the magma ocean. It may take a form of overturn as suggested for Mars by Elkins-Tanton et al. (2005), which would create a subadiabatic and gravitationally stable mantle. It should be emphasized that this remains one of the most difficult and uncertain aspects of magma ocean crystallization.

9.04.9 The Last Stages of Crystallization

9.04.9.1 Cessation of Suspension

The first important transition occurs when the molten layer disappears, that is, the potential temperature drops below liquidus everywhere. The crystal size increases because the sequence 'nucleation–growth–dissolution' changes to just 'growth.' During the nucleation–growth–dissolution cycle, the time available for Ostwald ripening is controlled by the residence time of crystals in the partially molten region, which is of the order of $t_{ost} \sim 3H/u_0 \sim 10^6$ s or roughly 1 week. When the completely molten layer disappears, crystals never exit the

two-phase region and the characteristic time for crystal growth is much larger. It can approximately be estimated as the time it takes for the potential temperature to drop from the liquidus temperature to the critical temperature for the rheological transition (i.e., while liquid-state convection still occurs). Since the difference between liquidus T_{liq} and solidus T_{sol} is about 600 K near the surface (Figure 1) and $\phi \approx 60\%$ is reached approximately in the middle between liquidus and solidus (Figure 2), then $t'_{ost} \sim 3 \times 10^9$ s (100 years) according to eqn [43]. The crystal size increases by $(t'_{ost}/t_{ost})^{1/3} \sim 14$ times, that is, $d'_{ost} \sim 10^{-2}$ m. If crystal–melt segregation did not start earlier, at this stage, it is impossible to avoid (Figure 8).

In addition, the surface temperature would eventually drop below 1500 K (Figure 4). If substantial amounts of water were present at that time, the atmosphere would change from silicate to steam one. The blanketing effect of the steam atmosphere can reduce the heat flux to 10^2–10^3 W m^{-2} (Abe and Matsui, 1986; Kasting, 1988; Zahnle et al., 1988). This would increase the crystal size even further and at the same time substantially reduce the ability of convection to suspend crystals (Figure 8).

The pressure at the bottom of the partially molten layer (the complete crystallization front) at the time when the completely molten layer disappears can be estimated from an adiabat, which starts at the liquidus temperature at the surface. The bottom of the partially molten layer is the pressure where this adiabat intersects with the solidus. It depends strongly on the details of the thermodynamics of the partially molten layer. Calculations by Miller et al. (1991a,b), Solomatov and Stevenson (1993b), Abe (1997), and Solomatov (2000) (Figures 1 and 3) suggest that the bottom of the partially molten layer is around 30–40 GPa.

When crystal–melt segregation begins, convection can become quite complex. This regime is poorly understood. It may develop layers and instabilities as experiments on convective suspension show (e.g., Koyaguchi et al., 1993; Sparks et al., 1993). Although convection is suppressed by sedimentation, it may not necessarily cease. Crystal fraction near the surface is below 60%, and thus, the viscosity in a thin region below the surface is still small. This might be sufficient to maintain convection at least in this layer. Note that convection is driven by the instabilities of the 1 cm thick surface thermal boundary layer and the heat flux does not depend much on the processes at large depth, such as crystal–melt segregation. This means that as long as a low-viscosity layer exists below the surface, one might expect that this layer would continue to convect vigorously generating the high heat flux predicted by eqns [19] and [21].

9.04.9.2 Formation of Thin Crust Within the Thermal Boundary Layer

Even though a low-viscosity region may exist below the surface, a stable crust can form within the thin thermal boundary layer, which would reduce the heat flux. Indeed, when the potential temperature drops below the liquidus, the surface temperature can reach the critical one where the crystal fraction is about 60% and can even reach the solidus (Figures 1, 2, and 4). First, it seems that it is unlikely that a solid or partially solid crust can form on the timescale of $\delta^2/4\kappa \sim 30$ s – this is too short for crystals to nucleate or grow. Second, if a rigid crust does form on top of the thermal boundary layer, its effect on the heat flux is not as big as one might expect. This can be estimated as follows. The viscosity decreases within the thermal boundary layer due to both temperature and crystal fraction. As a result, while the whole boundary layer cannot participate in convection because of the rigid crust, the bottom part which has the lowest viscosity can. This convection regime is called stagnant lid convection.

The heat flux in the stagnant lid convection regime can approximately be described by eqns [19] and [21], provided the temperature difference $T_m - T_s$ is replaced by the rheological temperature scale (Davaille and Jaupart, 1993a,b; Fowler, 1985; Morris and Canright, 1984; Solomatov, 1995a; Solomatov and Moresi, 2000). For magma, it is calculated as follows (Davaille and Jaupart, 1993b; Reese and Solomatov, 2006):

$$\Delta T_{rh} \approx 2\left|\frac{\mathrm{d}\ln\eta}{\mathrm{d}T}\right|^{-1}_{T=T_m} = 2\left|\frac{\partial\ln\eta}{\partial T} + \frac{\partial\ln\eta}{\partial\phi}\frac{\mathrm{d}\phi}{\mathrm{d}T}\right|^{-1}_{T=T_m} \quad [60]$$

Assuming an Arrhenius-dependence of melt viscosity on temperature, $\eta_l \sim \exp(E_l/RT)$, where the activation energy $E_l = 190$ kJ mol^{-1} (Liebske et al., 2005b) and using eqn [17] and Figure 2, we obtain that near liquidus $\Delta T_{rh} \approx 100$ K. This scale is mostly determined by the variation in the crystal fraction within the boundary layer.

Thus, the driving temperature difference for convection can be reduced by a factor of 2–6 compared to the temperature difference without solid crust (Figure 4) and the heat flux can drop by one order of magnitude (eqns [19] and [21]).

9.04.9.3 Cessation of Liquid-State Convection

When the crystal fraction increases to 60% all the way to the surface, the effective viscosity of magma is controlled by solid-state deformation of crystals. Convection becomes much slower, the heat flux drops, and a thick crust forms at the surface. The location of the bottom of the remaining partially molten layer can be obtained from an adiabat starting at the critical temperature for the rheological transition. Figure 1 suggests that such an adiabat intersects the solidus around 10 GPa or 300 km. This estimate is rather uncertain since even a 100 K error in the estimate of the rheological transition increases this pressure by a factor of 2. A similar factor can be caused by variations in the solidus and in the thermodynamics of partial melt. Also, this gives only a lower limit because the temperatures can be somewhat superadiabatic due to the strong variation of the viscosity with depth and because of the compositional stratification at shallow depth. After solid-state convection replaces liquid-state convection, percolation of melt through the solid matrix becomes an important process.

9.04.9.4 Percolation

Melt extraction from the remaining partially molten layer can be controlled by either the percolation of melt through the solid matrix or the compaction of the solid matrix (Bercovici et al., 2001; McKenzie, 1984). The compaction length is of the order of meters, which is much smaller than the depth L' of the remaining partially molten layer. This implies that compaction does not effect melt extraction and the rate-limiting process is

melt percolation. Although the melt fraction and the viscosities of solid and liquid vary in the partially molten region, an order-of-magnitude melt percolation time is

$$t_{\text{diff}} \sim \frac{L'}{u_{\text{perc}}} \quad [61]$$

where

$$u_{\text{perc}} = \frac{g\Delta\rho d^2 \phi_{\text{l}}^2}{150\eta_{\text{l}}(1-\phi_{\text{l}})} \quad [62]$$

is the percolation velocity (Dullien, 1979; Soo, 1967), which is related to Darcy velocity, $u_{\text{D}} \approx \phi_{\text{l}} u_{\text{perc}}$, and $\phi_{\text{l}} = 1 - \phi$ is the melt fraction. Melt is likely to migrate very quickly at the initial stages of percolation (near the rheological transition), when the melt fraction is large and the melt viscosity is low, and significantly slow down near the solidus when only a few percent melt is left. For $\phi_{\text{l}} \sim 2\%$, $d \sim 1\,\text{mm}$ and $\eta_{\text{l}} \sim 100\,\text{Pa s}$ (the value of the viscosity of a low-pressure, high silica, polymerized magma just above the solidus, Kushiro, 1980, 1986),

$$t_{\text{diff}} \sim 10^8 \left(\frac{\phi_{\text{l}}}{0.02}^2\right) \left(\frac{d}{10^{-3}\,\text{m}}\right)^2 \left(\frac{\eta_{\text{l}}}{100\,\text{Pa s}}\right) \text{years} \quad [63]$$

9.04.9.5 Crystal–Melt Density Inversions

Crystal–melt density inversions in the magma ocean (Agee, 1998) might result in the formation of more than one molten layer. This is very important because it determines the direction of melt migration and chemical differentiation in the magma ocean. It is now realized that stable molten layers could have been formed not only near the surface but also in the deep mantle, in the upper mantle, and at the core–mantle boundary (Agee, 2008; Akins et al., 2004; de Koker et al., 2013; Matsukage et al., 2005; Murakami and Bass, 2011; Nomura et al., 2011; Ohtani, 2009; Ohtani and Maeda, 2001; Stixrude and Karki, 2005). Constraining these density inversions is quite challenging and the results from different groups sometimes differ (e.g., Andrault et al., 2012). Besides the experimental difficulties, there are intrinsic difficulties in determining density inversions because of their high sensitivity to composition and, in particular, to poorly constrained iron and water contents in the melt.

Formation and evolution of a dense magmatic layer at the base of the mantle early in the Earth's history would have important consequences for the Earth's evolution (Labrosse et al., 2007). This layer can produce a hidden geochemical reservoir, which can be a host to various incompatible elements. For example, it can explain the apparent deficit of ^{40}K and the low degassing rates of ^{40}Ar and the difference in ^{142}Nd/^{144}Nd ratios between chondrites and the Earth's mantle. It can also explain He and Ne signatures of ocean island basalts (Coltice et al., 2011).

9.04.9.6 Remelting due to Melt Extraction

The extraction of melt is accompanied by gravitational energy release, which is converted to heat via viscous dissipation associated with melt migration. Assuming that most of the energy goes to melting, Solomatov and Stevenson (1993b) showed that the additional amount of melt generated is proportional to

$$R_{\text{m}} = \frac{\Delta\rho g L'}{\rho \Delta H} \quad [64]$$

The value of R_{m} is only about 0.1 for 50 km deep magma chambers but close to unity for a layer of $L' \sim 500\,\text{km}$ depth. Thus, the total degree of melting can roughly be twice as much as the initial degree of melting before melt extraction.

9.04.9.7 Solid-State Convection

The timescale for complete crystallization of the mantle depends on the style of convection in the remaining partially molten layers. When the deformation is controlled by solid-state creep, the heat flux is determined by the equations, which are similar to those describing plate tectonics. In its simplest form, it can be written as (Davies, 1990; Turcotte and Schubert, 2002)

$$F = 0.3k(T_{\text{m}} - T_{\text{s}})^{4/3} \left(\frac{\alpha\rho g}{\kappa\eta_{\text{s}}}\right)^{1/3} \quad [65]$$

For the viscosity $\eta_{\text{s}} \sim 10^{18}\,\text{Pa s}$, and the temperature difference across the surface thermal boundary layer $T_{\text{m}} - T_{\text{s}} \sim 1500\,\text{K}$ (i.e., the surface temperature is around 300 K), the earlier equation gives $F \sim 1\,\text{W m}^{-2}$. The thickness of the thermal boundary layer is about 1 km. The crystallization of a partially molten upper layer of thickness $L' \sim 500\,\text{km}$ takes

$$t_{\text{conv}} \sim \frac{\Delta H(1-\phi_{\text{m}})\rho L'}{F} \sim 10\,\text{Myr} \quad [66]$$

If one assumes that the surface layer is rigid and convection occurs in the stagnant lid regime, then the driving temperature $T_{\text{m}} - T_{\text{s}} \approx 1500\,\text{K}$ in eqn [65] needs to be replaced by the rheological temperature scale eqn [60]. Equations [60] and [18] give $\Delta T_{\text{rh}} \approx 100\,\text{K}$, where we assumed $\text{d}\phi/\text{d}T \approx 5 \times 10^{-4}\,\text{K}^{-1}$ near the rheological transition (the melt fraction is about 40%; **Figure 2**) and $E \approx 240\,\text{kJ mol}^{-1}$, which is the activation energy for diffusion creep in water-saturated olivine (Karato and Wu, 1993). The heat flux can drop by a factor of ~ 40, thus increasing the crystallization time to $\sim 400\,\text{Myr}$. If the viscosity η_{s} and/or $\text{d}\phi/\text{d}T$ is larger (the latter depends on the details of the phase diagram), the crystallization time can increase further, perhaps, to 2 billion years or so.

It is also possible that density stratification due to chemical differentiation completely suppresses convection. In the stagnant lid convection regime, where the driving temperature differences are small, this does not take much (Zaranek and Parmentier, 2004). If this happens, cooling and crystallization would be controlled by thermal diffusion whose timescale $\sim L'^2/4\kappa$ is about 2 billion years. These order-of-magnitude estimates show the crystallization time can be comparable with the age of the Earth. This means that it is possible that the Earth never had a chance to crystallize completely.

The early studies inevitably considered a simple, one-dimensional model of magma ocean crystallization in which any chemical heterogeneities would form laterally homogeneous layers. However, the mantle may acquire lateral heterogeneities as well, for example, because of an asymmetrical pattern

of impact-induced melting and incomplete mixing. Smaller, yet still sufficiently large impacts capable of melting a part of the mantle may produce localized magma oceans, which form lateral heterogeneities (Reese et al., 2007b). These heterogeneities are likely to be not only chemical but also rheological and would be difficult to mix by mantle convection later in the Earth's history (Solomatov and Reese, 2008). A growing number of isotopic evidence do indeed suggest that early differentiation of the Earth was heterogeneous and these heterogeneities may have never fully mixed by mantle convection (Bennett et al., 2008; Caro, 2011; Touboul et al., 2012).

9.04.10 Magma Oceans on Other Planets

The magma ocean hypothesis is becoming an important building block in the narrative of the formation and evolution of not only the Earth but also other planets (Albarède and Blichert-Toft, 2007; Brown and Elkins-Tanton, 2009; Elkins-Tanton, 2012; Elkins-Tanton et al., 2005; Reese and Solomatov, 2006; Reese et al., 2007a; Sleep, 2000; Stevenson, 2008; Zahnle et al., 2007).

Venus is similar in size to Earth and is likely to have undergone some form of widespread melting. The extent of melting and the evolution of the Venusian magmasphere can be very different from the Earth because of the stochastic nature of the formation process. The Venusian magmasphere may have lasted longer and could have even expanded during the Venusian history due to radioactive heating and inefficient cooling in the absence of plate tectonics (Reese et al., 2007a). This may explain the extensive volcanism in the past billion years or so and the existence of recent (within a few million years) volcanism (Smrekar et al., 2010).

Mars is roughly half the size of the Earth and seems to have differentiated fast. The estimates range from around a few tens of millions of years (Foley et al., 2005; Kleine et al., 2002) to a few millions of years (Dauphas and Pourmand, 2011). The small size of Mars and the isotopic data suggest more localized magma oceans leading to a more heterogeneous planet (Reese and Solomatov, 2006; Reese et al., 2007b). This type of magma oceans is in contrast to a global, more or less uniform magma ocean usually assumed for the Earth.

Mercury has a peculiar structure characterized by an extremely thin mantle. A giant impact has been proposed as one of the possible causes (Benz et al., 1988). More recently, the magma ocean hypothesis has been invoked to explain the observed low-iron content of the crust by a postcrystallization mantle overturn (Brown and Elkins-Tanton, 2009).

Although Io, Jupiter's satellite, has been known for its extraordinary level of volcanism caused by tidal heating, the possibility that Io may have a global magma ocean has been suggested only recently (Khurana et al., 2011). A partially molten layer with thickness of about 50 km and 20% melt seems to explain best the magnetic data returned by the Galileo mission.

Isotopic data suggest that even small bodies underwent melting and differentiation early during planetary formation. High-precision Hf–W data for iron meteorites suggest that this happened in about 1–1.5 million years (Kruijer et al., 2012; Qin et al., 2008; Scherstén et al., 2006). It is important to note that the estimates of differentiation times assume equilibrium melting. Impact-induced metal/silicate segregation may have occurred under nonequilibrium conditions (Tomkins et al., 2013). If so, this implies that the time might be longer than the equilibrium model suggest and that melting may have been caused by impacts rather than by ^{26}Al.

The growing list of planets outside of the solar system now includes planets that are currently likely to be at least partially molten. For example, CoRoT-7b, about 500 light years away from Earth and about 1.7 times the size of Earth, is estimated to be melted due to tidal heating and its proximity to the star, which keeps its surface temperature around 1800–2600 K (Léger et al., 2009). A more recently discovered Kepler-10b, which is 560 light years away from Earth and is closer in size to Earth (about 1.4 times larger), also has a very hot surface, around 1800 K.

9.04.11 Summary

Crystallization of the molten Earth was undoubtedly very complex. A variety of physical and chemical processes determined the final product of crystallization during the first 10^8 years, before the long-term solid-state convection took over. This includes convection in liquid, solid, and partially molten states, crystal settling during the early stages of crystallization, and extraction of residual melt from the partially molten mantle during the later stages.

A scenario that seems to agree with the geochemical constraints and is physically feasible is as follows. The latest and the largest impact melts a significant part of the Earth. Gravitational instabilities quickly redistribute the material so that denser materials (due to temperature and composition) accumulate at the bottom and lighter ones accumulate at the top. A small fraction of the mantle that survived the impact and remained solid sink to the bottom of the magma ocean.

In the beginning, the viscosity of the magma ocean is very low ($\sim$0.1 Pa s), the magma ocean is vigorously convecting, and the heat flux $\sim 10^6$ W m^{-2}. The temperature profile is approximately adiabatic. Since the melting curve is likely to be steeper than the adiabat, crystallization proceeds from the bottom up. It takes about $\sim 10^3$ years to crystallize the lower part of the mantle. Highly turbulent convection helps to cool and crystallize the magma ocean to about 60% crystal fraction (the rheological transition from a low-viscosity suspension to a high-viscosity partially molten solid).

Whether or not fractional crystallization is prevented during the early stages of crystallization depends on the crystal size. It is controlled by nucleation in the downgoing convective flow and by Ostwald ripening. The crystal diameter established by these processes can be sufficiently small ($\sim$1 mm) to allow equilibrium crystallization. The lower part of the mantle underwent only a small degree of crystal–melt segregation, which can be reconciled with the geochemical constrained on the fractionation of minor and trace elements.

Crystallization beyond the crystal fraction of 60% is accomplished by solid-state creep convection. Although the viscosity of solids is very high ($\sim 10^{18}$ Pa s at the solidus and $\sim 10^{14}$ Pa s near 60% crystal fraction), convection remains sufficiently fast and is able to help crystallize the lower mantle completely.

Several important changes happen during the last stages of crystallization of the magma ocean. The purely molten region disappears, and the crystals undergo continuous growth rather

than cycle between nucleation, growth, and dissolution. The early silicate atmosphere changes to a steam atmosphere whose blanketing effect can reduce the heat flux by several orders of magnitude. Convection becomes weaker, while the crystals grow larger and cannot be suspended by convection. Crystal settling or flotation (depending on pressure) creates a compositional and density stratification, which tends to suppress convection although vigorous convection and cooling are likely to continue near the surface. When the crystal fraction reaches the maximum packing fraction of about $\sim$60% all the way to the surface, the heat flux drops to $\sim 1\ \mathrm{W\,m^{-2}}$ because of the viscosity jump from liquid-like to solid-like viscosity (the rheological transition). Formation of the solid crust can reduce the heat flux further by one order of magnitude. All these changes contribute to the onset of crystal–melt segregation in the magma ocean. The depth of the differentiated region is from a few hundred kilometers to 1000 km, with the melt fraction varying from zero at the bottom to $\sim$60% at the top.

Crystallization of this remaining partially molten layer takes 10^7–10^9 years, depending on the regime of mantle convection (surface recycling or stagnant lid convection). This is comparable with the time it takes the melt to escape via percolation. Radiogenic heating and subsolidus convection become the main factors determining the subsequent evolution of the planet.

The two very different timescales, 10^3 years for crystallization of the lower mantle and 10^7–10^9 years for crystallization of the upper mantle, suggest that whenever the Earth was melted by a giant impact, the lower mantle healed very quickly, while the upper mantle never had enough time to crystallize completely. If so, then iron delivered by impacts accumulated at the base of the upper mantle before it sank into the Earth's core. Thus, chemical equilibrium between iron and silicates was established at high pressures near the bottom of the partially molten upper mantle in agreement with models of abundances of siderophile elements.

Although the model of equilibrium crystallization provides a simple conceptual framework that can help to reconcile various geochemical constraints, some form of fractional crystallization cannot be excluded within the uncertainties of physical parameters. Also, fractional crystallization is inevitable at some stage of crystallization even within this model. The dynamics of fractional crystallization is undoubtedly very complex and involves a variety of dynamic processes including crystal settling/flotation, convective mixing in the melt and in the partially molten solid, melt percolation, gravitational instabilities due to unstable density stratification, and compositional and convective layering. This is an important problem that needs to be addressed in the future. Finally, future studies will need to consider primordial differentiation of the Earth's mantle in combination with planetary accretion, core formation, and atmospheric evolution.

References

Abe Y (1993) Physical state of the very early Earth. *Lithos* 30: 223–235.

Abe Y (1995) Early evolution of the terrestrial planets. *Journal of Physics of the Earth* 43: 515–532.

Abe Y (1997) Thermal and chemical evolution of the terrestrial magma ocean. *Physics of the Earth and Planetary Interiors* 100: 27–39.

Abe Y (2011) Protoatmospheres and surface environment of protoplanets. *Earth, Moon, and Planets* 108: 9–14.

Abe Y and Matsui T (1986) Early evolution of the Earth: Accretion, atmosphere formation, and thermal history. *Journal of Geophysical Research* 91: E291–E302.

Abe Y, Ohtani E, Okuchi T, Righter K, and Drake M (2000) Water in the early Earth. In: Canup RM and Righter K (eds.) *Origin of the Earth and Moon*, pp. 413–433. Tucson, AZ: University of Arizona Press.

Adjaoud O, Steinle-Neumann G, and Jahn S (2012) Transport properties of Mg_2SiO_4 liquid at high pressure: Physical state of a magma ocean. *Earth and Planetary Science Letters* 312: 463–470.

Agee CB (1990) A new look at differentiation of the Earth from melting experiments on the Allende meteorite. *Nature* 346: 834–837.

Agee CB (1998) Crystal-liquid density inversions in terrestrial and lunar magmas. *Physics of the Earth and Planetary Interiors* 107: 63–74.

Agee CB (2008) Static compression of hydrous silicate melt and the effect of water on planetary differentiation. *Earth and Planetary Science Letters* 265: 641–654.

Agee CB and Walker D (1988) Mass balance and phase density constraints on early differentiation of chondritic mantle. *Earth and Planetary Science Letters* 90: 144–156.

Ahrens TJ (1992) A magma ocean and the Earth's internal water budget. In: Agee CB and Longhi J (eds.) *Workshop on the Physics and Chemistry of Magma Oceans from 1 bar to 4 Mbar, LPI Tech. Rep. 92-03*, pp. 13–14. Houston: Lunar and Planetary Institute.

Akins JA, Luo SN, Asimow PD, and Ahrens TJ (2004) Shock-induced melting of $MgSiO_3$ perovskite and implications for melts in Earth's lowermost mantle. *Geophysical Research Letters* 31. http://dx.doi.org/10.1029/2004GL020237.

Albarède F and Blichert-Toft J (2007) The split fate of the early Earth, Mars, Venus, and Moon. *Comptes Rendus Geoscience* 339: 917–927.

Albarède F, Blichert-Toft J, Vervoort JD, Gleason JD, and Rosing M (2000) Hf–Nd isotope evidence for a transient dynamic regime in the early terrestrial mantle. *Nature* 404: 488–490.

Amelin Y, Lee DC, Halliday AN, and Pidgeon RT (1999) Nature of the Earth's earliest crust from hafnium isotopes in single detrital zircons. *Nature* 399: 252–255.

Andrade ENC (1952) Viscosity of liquids. *Proceedings of the Royal Society of London, Series A* 215: 36–43.

Andrault D, Petitgirard S, Lo Nigro G, et al. (2012) Solid-liquid iron partitioning in Earth's deep mantle. *Nature* 487: 354–359.

Arzi AA (1978) Critical phenomena in the rheology of partially melted rocks. *Tectonophysics* 44: 173–184.

Asimow PD, Hirschmann MM, and Stolper EM (1997) An analysis of variations in isentropic melt productivity. *Philosophical Transactions of the Royal Society of London, Series A* 355: 255–281.

Bartlett RB (1969) Magma convection, temperature distribution, and differentiation. *American Journal of Science* 267: 1067–1082.

Béjina F, Jaoul O, and Liebermann RC (2003) Diffusion in minerals at high pressure: A review. *Physics of the Earth and Planetary Interiors* 139: 3–20.

Bennett VC, Brandon AD, and Nutman AP (2008) Coupled ^{142}Nd–^{143}Nd isotopic evidence for Hadean mantle dynamics. *Science* 318: 1907–1910.

Bennett VC, Nutman AP, and McCulloch MT (1993) Nd isotopic evidence for transient highly-depleted mantle reservoirs in the early history of the Earth. *Earth and Planetary Science Letters* 119: 299–317.

Benz W and Cameron AGW (1990) Terrestrial effects of the giant impact. In: Newsom HE and Jones JH (eds.) *Origin of the Earth*, pp. 61–67. New York: Oxford University Press.

Benz W, Cameron AGW, and Melosh HJ (1989) The origin of the Moon and the single impact hypothesis, III. *Icarus* 81: 113–131.

Benz W, Slattery WL, and Cameron AGW (1986) The origin of the Moon and the single impact hypothesis, I. *Icarus* 66: 515–535.

Benz W, Slattery WL, and Cameron AGW (1987) The origin of the Moon and the single impact hypothesis, II. *Icarus* 71: 30–45.

Benz W, Slattery WL, and Cameron AGW (1988) Collisional stripping of Mercury's mantle. *Icarus* 74: 516–528.

Bercovici D, Ricard Y, and Schubert G (2001) A two-phase model for compaction and damage 1. General theory. *Journal of Geophysical Research* 106: 8887–8906.

Bizzarro M, Baker JA, Haack H, Ulfbeck D, and Rosing MG (2003) Early history of Earth's crust–mantle system inferred from hafnium isotopes in chondrites. *Nature* 421: 931–933.

Boehler R (1992) Melting of the Fe–FeO and the Fe–FeS systems at high pressure: Constraints on core temperatures. *Earth and Planetary Science Letters* 111: 217–227.

Boehler R (1996) Melting temperature of the Earth's mantle and core: Earth's thermal structure. *Annual Review of Earth and Planetary Sciences* 24: 15–40.

Boehler R (2000) High-pressure experiments and the phase diagram of lower mantle and core materials. *Reviews of Geophysics* 38: 221–245.

Bottinga Y, Richet P, and Sipp A (1995) Viscosity regimes of homogeneous silicate melts. *American Mineralogist* 80: 305–318.

Bottinga Y and Weill DF (1972) The viscosity of magmatic silicate liquids: A model for calculation. *American Journal of Science* 272: 438–475.

Boubnov BM and Golitsyn GS (1986) Experimental study of convective structures in rotating fluids. *Journal of Fluid Mechanics* 167: 503–531.

Boubnov BM and Golitsyn GS (1990) Temperature and velocity field regimes of convective motions in a rotating plane fluid layer. *Journal of Fluid Mechanics* 219: 215–239.

Bowring SA and Housh T (1995) The Earth's early evolution. *Science* 269: 1535–1540.

Boyet M and Carlson RW (2005) ^{142}Nd evidence for early (>4.53 Ga) global differentiation of the silicate Earth. *Science* 309: 576–581.

Brinkman HC (1952) The viscosity of concentrated suspensions and solutions. *Journal of Chemical Physics* 20: 571–581.

Brown S and Elkins-Tanton LT (2009) Compositions of Mercury's earliest crust from magma ocean models. *Earth and Planetary Science Letters* 286: 446–455.

Buyevich YA and Mansurov VV (1991) Kinetics of the intermediate stage of phase transition in batch crystallization. *Journal of Crystal Growth* 104: 861–867.

Cameron AGW (1997) The origin of the Moon and the single impact hypothesis V. *Icarus* 126: 126–137.

Campbell GA and Forgacs G (1990) Viscosity of concentrated suspensions: An approach based on percolation theory. *Physical Review A* 41: 4570–4573.

Canup RM (2004) Simulations of a late lunar-forming impact. *Icarus* 168: 433–456.

Canup RM (2008) Accretion of the Earth. *Philosophical Transactions of the Royal Society A* 366: 4061–4075.

Canup RM and Agnor CB (2000) Accretion of the terrestrial planets and the Earth–Moon system. In: Canup RM and Righter K (eds.) *Origin of the Earth and Moon*, pp. 113–129. Tucson, AZ: University of Arizona Press.

Canup RM and Asphaug E (2001) Origin of the Moon in a giant impact near the end of the Earth's formation. *Nature* 412: 708–712.

Canup RM and Esposito LW (1996) Accretion of the Moon from an impact-generated disk. *Icarus* 119: 427–446.

Canuto VM and Dubovikov MS (1998) Two scaling regimes for rotating Rayleigh–Benard convection. *Physical Review Letters* 80: 281–284.

Caro G (2011) Early silicate Earth differentiation. *Annual Review of Earth and Planetary Sciences* 39: 31–58.

Caro G, Bourdon B, Birck JL, and Moorbath S (2003) ^{146}Sm–^{142}Nd evidence from Isua metamorphosed sediments for early differentiation of the Earth's mantle. *Nature* 423: 428–432.

Caro G, Bourdon B, Wood BJ, and Corgne A (2005) Trace-element fractionation in Hadean mantle generated by melt segregation from a magma ocean. *Nature* 436: 246–249.

Cashman KV (1993) Relationship between plagioclase crystallization and cooling rate in basaltic melts. *Contributions to Mineralogy and Petrology* 113: 126–142.

Cashman KV and Marsh BD (1988) Crystal size distribution (CSD) in rocks and the kinetics and dynamics of crystallization II. Makaopuhi lava lake. *Contributions to Mineralogy and Petrology* 99: 292–305.

Castaing B, Gunaratne G, Heslot F, et al. (1989) Scaling of hard thermal turbulence in Rayleigh–Benard convection. *Journal of Fluid Mechanics* 204: 1–30.

Caughey SJ and Palmer SG (1979) Some aspects of turbulence structure through the depth of the convective boundary layer. *Quarterly Journal of the Royal Meteorological Society* 105: 811–827.

Chambers JE and Wetherill GW (1998) Making the terrestrial planets: N-body integrations of planetary embryos in three dimensions. *Icarus* 136: 304–327.

Chen R, Fernando HJS, and Boyer DL (1989) Formation of isolated vortices in a rotating convecting fluid. *Journal of Geophysical Research* 94: 18445–18453.

Clark SP (1957) Radiative transfer in the Earth's mantle. *Transactions of the American Geophysical Union* 38: 931–938.

Collerson KD, Campbell LM, Weaver BL, and Palacz ZA (1991) Evidence for extreme mantle fractionation in early Archaean ultramafic rocks from northern Labrador. *Nature* 349: 209–214.

Coltice N, Moreira M, Hernlund J, and Labrosse S (2011) Crystallization of a basal magma ocean recorded by helium and neon. *Earth and Planetary Science Letters* 308: 193–199.

Cooper RF and Kohlstedt DL (1986) Rheology and structure of olivine-basalt partial melts. *Journal of Geophysical Research* 91: 9315–9323.

Corgne A, Liebske C, Wood BJ, Rubie DC, and Frost DJ (2005) Silicate perovskite-melt partitioning of trace elements and geochemical signature of a deep perovskitic reservoir. *Geochimica et Cosmochimica Acta* 69: 485–496.

Corgne A and Wood BJ (2002) $CaSiO_3$ and $CaTiO_3$ perovskite-melt partitioning of trace elements: Implications for gross mantle differentiation. *Geophysical Research Letters* 29. http://dx.doi.org/10.1029/2001GL014398.

Costa A (2005) Viscosity of high crystal content melts: Dependence on solid fraction. *Geophysical Research Letters* 32. http://dx.doi.org/10.1029/2005GL024303.

Dauphas N and Pourmand A (2011) Hf-W-Th evidence for rapid growth of Mars and its status as a planetary embryo. *Nature* 473: 489–493.

Davaille A and Jaupart C (1993a) Transient high Rayleigh number thermal convection with large viscosity variations. *Journal of Fluid Mechanics* 253: 141–166.

Davaille A and Jaupart C (1993b) Thermal convection in lava lakes. *Geophysical Research Letters* 20: 1827–1830.

Davies GF (1990) Heat and mass transport in the early Earth. In: Newsom HE and Jones JH (eds.) *Origin of the Earth*, pp. 175–194. New York: Oxford University Press.

Davis RH and Acrivos A (1985) Sedimentation of noncolloidal particles at low Reynolds numbers. *Annual Review of Fluid Mechanics* 17: 91–118.

de Koker N, Karki BB, and Stixrude L (2013) Thermodynamics of the MgO–SiO_2 liquid system in Earth's lowermost mantle from first principles. *Earth and Planetary Science Letters* 361: 58–63.

de Koker N and Stixrude L (2009) Self-consistent thermodynamic description of silicate liquids, with application to shock melting of MgO periclase and $MgSiO_3$ perovskite. *Geophysical Journal International* 178: 162–179.

Deardorff JW (1970) Convective velocity and temperature scales for the unstable planetary boundary layer and for Rayleigh convection. *Journal of Atmospheric Science* 27: 1211–1213.

Dingwell DB, Courtial P, Giordano D, and Nichols ARL (2004) Viscosity of peridotite liquid. *Earth and Planetary Science Letters* 226: 127–138.

Dowty E (1980) Crystal growth and nucleation theory and the numerical simulation of igneous crystallization. In: Hargraves RV (ed.) *Physics of Magmatic Processes*, pp. 419–485. Princeton: Princeton University Press.

Drake MJ (2000) Accretion and primary differentiation of the Earth: A personal journey. *Geochimica et Cosmochimica Acta* 64: 2363–2370.

Dullien FAL (1979) *Porous Media: Fluid Transport and Pore Structure*. San Diego, CA: Academic Press.

Einstein A (1906) Eine neue Bestimmung der Moleküldimensionen. *Annalen der Physik* 19: 289–306.

Elkins-Tanton LT (2011) Linked magma ocean solidification and atmospheric growth for Earth and Mars. *Earth and Planetary Science Letters* 271: 181–191.

Elkins-Tanton LT (2012) Magma oceans in the inner Solar System. *Annual Review of Earth and Planetary Sciences* 40: 113–139.

Elkins-Tanton LT, Zaranek SE, Parmentier EM, and Hess PC (2005) Early magnetic field and crust on Mars from magma ocean cumulate overturn. *Earth and Planetary Science Letters* 236: 1–12.

Elsasser WM (1963) Early history of the Earth; dedicated to F. G. Houtermans on his sixtieth birthday. In: Geiss J and Goldberg ED (eds.) *Earth Science and Meteoritics*, pp. 1–30. Amsterdam: North-Holland.

Fernando HJS, Chen RR, and Boyer DL (1991) Effects of rotation on convective turbulence. *Journal of Fluid Mechanics* 228: 513–547.

Flasar FM and Birch F (1973) Energetics of core formation: A correction. *Journal of Geophysical Research* 78: 6101–6103.

Flemings MC, Riek RG, and Young KP (1976) Rheocasting. *Materials Science and Engineering* 25: 103–117.

Foley CN, Wadhwa M, Borg LE, Janney PE, Hines R, and Grove TL (2005) The early differentiation history of Mars from W-182–Nd-142 isotope systematics in the SNC meteorites. *Geochimica et Cosmochimica Acta* 69: 4557–4571.

Fowler AC (1985) Fast thermoviscous convection. *Studies in Applied Mathematics* 72: 189–219.

Frankel NA and Acrivos A (1967) On the viscosity of a concentrated suspension of solid spheres. *Chemical Engineering Science* 22: 847–853.

Gans RF (1972) Viscosity of the Earth's core. *Journal of Geophysical Research* 77: 360–366.

Gasparik T and Drake MJ (1995) Partitioning of elements among two silicate perovskites, superphase B, and volatile-bearing melt at 23 GPa and 1500–1600 °C. *Earth and Planetary Science Letters* 134: 307–318.

German RM (1985) *Liquid Phase Sintering*. New York: Plenum Press.

Ghiorso MS (1997) Thermodynamic models of igneous processes. *Annual Review of Earth and Planetary Sciences* 25: 221–241.

Glazier JA (1999) Evidence against 'ultrahard' thermal turbulence at very high Rayleigh numbers. *Nature* 398: 307–310.

Golitsyn GS (1980) Geostrophic convection. *Doklady Akademii Nauk SSSR* 251: 1356–1360.

Golitsyn GS (1981) Structure of convection in rapid rotation. *Doklady Akademii Nauk SSSR* 261: 317–320.

Goody RM (1995) *Principles of Atmospheric Physics and Chemistry*. New York: Oxford University Press.

Grossmann S and Lohse D (1992) Scaling in hard turbulent Rayleigh–Bènard flow. *Physical Review A* 46: 903–917.
Grove TL (1990) Cooling histories of lavas from Serocki volcano. In: *Proceedings of the Ocean Drilling Program, 106/109,* pp. 3–8.
Grove TL and Walker D (1977) Cooling histories of Apollo 15 quartz-normative basalts. In: *Proceedings of the 8th Lunar and Planetary Science Conference*, pp. 1501–1520.
Halliday AN (2004) Mixing, volatile loss and compositional change during impact-driven accretion of the Earth. *Nature* 427: 505–509.
Halliday A, Rehkämper M, Lee D-C, and Yi W (1996) Early evolution of the Earth and Moon: New constraints from Hf–W isotope geochemistry. *Earth and Planetary Science Letters* 142: 75–89.
Harrison TM, Blichert-Toft J, Muller W, Albarède F, Holden P, and Mojzsis SJ (2005) Heterogeneous Hadean hafnium: Evidence of continental crust at 4.4 to 4.5 Ga. *Science* 310: 1947–1950.
Hayashi C, Nakazawa K, and Mizuno H (1979) Earth's melting due to the blanketing effect of the primordial dense atmosphere. *Earth and Planetary Science Letters* 43: 22–28.
Herzberg C and Gasparik T (1991) Garnet and pyroxenes in the mantle: A test of the majorite fractionation hypothesis. *Journal of Geophysical Research* 96: 16263–16274.
Hirose K, Shimizu N, van Westrenen W, and Fei Y (2004) Trace element partitioning in Earth's lower mantle and implications for geochemical consequences of partial melting at the core–mantle boundary. *Physics of the Earth and Planetary Interiors* 146: 249–260.
Hirth G and Kohlstedt DL (1995a) Experimental constraints on the dynamics of the partially molten upper mantle: Deformation in the diffusion creep regime. *Journal of Geophysical Research* 100: 1981–2001.
Hirth G and Kohlstedt DL (1995b) Experimental constraints on the dynamics of the partially molten upper mantle 2. Deformation in the dislocation creep regime. *Journal of Geophysical Research* 100: 15441–15449.
Holland KG and Ahrens TJ (1997) Melting of $(Mg,Fe)_2SiO_4$ at the core–mantle boundary of the Earth. *Science* 275: 1623–1625.
Hopfinger EJ (1987) Turbulence in stratified fluids: A review. *Journal of Geophysical Research* 92: 5287–5303.
Hopfinger EJ (1989) Turbulence and vortices in rotating fluids. In: Germain P, Piau M, and Caillerie D (eds.) *Theoretical and Applied Mechanics*, pp. 117–138. New York: Elsevier.
Hopfinger EJ, Browand FK, and Gagne Y (1982) Turbulence and waves in a rotating tank. *Journal of Fluid Mechanics* 125: 505–534.
Hostetler CJ and Drake MJ (1980) On the early global melting of the terrestrial planets. In: *Proceedings of the 11th Lunar and Planetary Science Conference,* pp. 1915–1929.
Huppert HE and Sparks RSJ (1980) The fluid dynamics of a basaltic magma chamber replenished by influx of hot, dense ultrabasic magma. *Contributions to Mineralogy and Petrology* 75: 279–289.
Ichikawa K, Kinoshita Y, and Shimamura S (1985) Grain refinement in Al–Cu binary alloys by rheocasting. *Transactions of the Japan Institute of Metals* 26: 513–522.
Ida S, Canup RM, and Stewart GR (1997) Lunar accretion from an impact-generated disk. *Nature* 389: 353–357.
Ita J and Cohen RE (1998) Diffusion in MgO at high pressure: Implications for lower mantle rheology. *Geophysical Research Letters* 25: 1095–1098.
Ito E, Kubo A, Katsura T, and Walter MJ (2004) Melting experiments of mantle materials under lower mantle conditions with implications for magma ocean differentiation. *Physics of the Earth and Planetary Interiors* 143: 397–406.
Ito E and Takahashi E (1987) Melting of peridotite at uppermost lower-mantle conditions. *Nature* 328: 514–517.
Jacobsen SB (2005) The Hf–W isotopic system and the origin of the Earth and Moon. *Annual Review of Earth and Planetary Sciences* 33: 531–570.
Jin Z-M, Green HW, and Zhou Y (1994) Melt topology in partially molten mantle peridotite during ductile deformation. *Nature* 372: 164–167.
Kadanoff LP (2001) Turbulent heat flow: Structures and scalings. *Physics Today* 54: 34–39.
Karato S-I and Li P (1992) Diffusion creep in perovskite: Implications for the rheology of the lower mantle. *Science* 255: 1238–1240.
Karato S-I and Murthy VR (1997a) Core formation and chemical equilibrium in the Earth – I. Physical considerations. *Physics of the Earth and Planetary Interiors* 100: 61–79.
Karato S-I and Murthy VR (1997b) Core formation and chemical equilibrium in the Earth – II. Chemical consequences for the mantle and core. *Physics of the Earth and Planetary Interiors* 100: 81–95.
Karato S-I and Wu P (1993) Rheology of the upper mantle: A synthesis. *Science* 260: 771–778.
Karki BB and Stixrude LP (2010) Viscosity of $MgSiO_3$ liquid at Earth's mantle conditions: Implications for an early magma ocean. *Science* 328: 740–742.
Kasting JF (1988) Runaway and moist greenhouse atmosphere and the evolution of Earth and Venus. *Icarus* 74: 472–494.
Kato T, Ringwood AE, and Irifune T (1988a) Experimental determination of element partitioning between silicate perovskites. garnets and liquids: Constraints on early differentiation of the mantle. *Earth and Planetary Science Letters* 89: 123–145.
Kato T, Ringwood AE, and Irifune T (1988b) Constraints on element partition coefficients between $MgSiO_3$ perovskite and liquid determined by direct measurements. *Earth and Planetary Science Letters* 90: 65–68.
Kaula WM (1979) Thermal evolution of earth and moon growing by planetesimals impacts. *Journal of Geophysical Research* 84: 999–1008.
Ke Y and Solomatov VS (2006) Early transient superplumes and the origin of the Martian crustal dichotomy. *Journal of Geophysical Research* 111. http://dx.doi.org/10.1029/2005JE002631.
Ke Y and Solomatov VS (2009) Coupled core–mantle thermal evolution of early Mars. *Journal of Geophysical Research* 114. http://dx.doi.org/10.1029/2008JE003291.
Khurana KK, Jia XZ, Kivelson MG, et al. (2011) Evidence of a global magma ocean in Io's interior. *Science* 332: 1186–1189.
King SD (1995) Models of mantle viscosity. In: Ahrens TJ (ed.) *Mineral Physics and Crystallography: A Handbook of Physical Constants*, pp. 227–236. Washington, DC: American Geophysical Union.
Kleine T, Münker C, Mezger K, and Palme H (2002) Rapid accretion and early core formation on asteroids and the terrestrial planets from Hf–W chronometry. *Nature* 418: 952–955.
Knittle E and Jeanloz R (1989) Melting curve of $(Mg, Fe)SiO_3$ perovskite to 96 GPa: Evidence for a structural transition in lower mantle melts. *Geophysical Research Letters* 16: 421–424.
Kohlstedt DL and Zimmerman ME (1996) Rheology of partially molten mantle rocks. *Annual Review of Earth and Planetary Sciences* 24: 41–62.
Koyaguchi T, Hallworth MA, and Huppert HE (1993) An experimental study of the effects of phenocrysts on convection in magmas. *Journal of Volcanology and Geothermal Research* 55: 15–32.
Kraichnan RH (1962) Turbulent thermal convection at arbitrary Prandtl number. *Physics of Fluids* 5: 1374–1389.
Krieger IM and Dougherty TJ (1959) A mechanism for non-Newtonian flow in suspensions of rigid spheres. *Transactions of the Society of Rheology* 3: 137–152.
Kruijer TS, Sprung P, Kleine T, et al. (2012) Hf-W chronometry of core formation in planetesimals inferred from weakly irradiated iron meteorites. *Geochimica et Cosmochimica Acta* 99: 287–304.
Kushiro I (1980) Viscosity, density, and structure of silicate melts at high pressures, and their petrological applications. In: Hargraves RB (ed.) *Physics of Magmatic Processes*, pp. 93–120. Princeton: Princeton University Press.
Kushiro I (1986) Viscosity of partial melts in the upper mantle. *Journal of Geophysical Research* 91: 9343–9350.
Labrosse S, Hernlund JW, and Coltice N (2007) A crystallizing dense magma ocean at the base of the Earth's mantle. *Nature* 450: 866–869.
Lee D-C and Halliday AN (1995) Hafnium–tungsten chronometry and the timing of terrestrial core formation. *Nature* 378: 771–774.
Léger A, Rouan D, Schneider J, et al. (2009) Transiting exoplanets from the CoRoT space mission. *Astronomy & Astrophysics* 506: 287–302.
Lejeune A-M and Richet P (1995) Rheology of crystal-bearing silicate melts: An experimental study at high viscosities. *Journal of Geophysical Research* 100: 4215–4229.
Li J and Agee CB (1996) Geochemistry of mantle–core differentiation at high pressure. *Nature* 381: 686–689.
Li P, Karato S, and Wang ZC (1996) High-temperature creep in fine-grained polycrystalline $CaTiO_3$, an analogue material of $(Mg,Fe)SiO_3$. *Physics of the Earth and Planetary Interiors* 95: 19–36.
Liebske C, Corgne A, Frost DJ, Rubie DC, and Wood BJ (2005a) Compositional effects on element partitioning between Mg-silicate perovskite and silicate melts. *Contributions to Mineralogy and Petrology* 149: 113–128.
Liebske C, Schmickler B, Terasaki H, et al. (2005b) Viscosity of peridotite liquid up to 13 GPa: Implications for magma ocean viscosities. *Earth and Planetary Science Letters* 240: 589–604.
Lifshitz IM and Slyozov VV (1961) The kinetics of precipitation from supersaturated solid solution. *Journal of Physics and Chemistry of Solids* 19: 35–50.
Lofgren G, Donaldson CH, Williams RJ, Mullins O, and Usselman TM (1974) Experimentally reproduced textures and mineral chemistry of Apollo 15 quartz-normative basalts. In: *Proceedings of the 5th Lunar Science Conference,* pp. 549–567.
Longhi J (1980) A model of early lunar differentiation. In: *Proceedings of the 11th Lunar Science Conference,* pp. 289–315.

Marcq E (2012) A simple 1-D radiative-convective atmospheric model designed for integration into coupled models of magma ocean planets. *Journal of Geophysical Research* 117. http://dx.doi.org/10.1029/2011JE003912.

Marsh BD and Maxey MR (1985) On the distribution and separation of crystals in convecting magma. *Journal of Volcanology and Geothermal Research* 24: 95–150.

Martin D and Nokes R (1988) Crystal settling in a vigorously convecting magma chamber. *Nature* 332: 534–536.

Martin D and Nokes R (1989) A fluid dynamical study of crystal settling in convecting magmas. *Journal of Petrology* 30: 1471–1500.

Matsui T and Abe Y (1986) Formation of a "magma ocean" on the terrestrial planets due to the blanketing effect of an impact-induced atmosphere. *Earth, Moon, and Planets* 34: 223–230.

Matsukage KN, Jing Z, and Karato S-I (2005) Density of hydrous silicate melt at the conditions of Earth's deep upper mantle. *Nature* 438: 488–491.

McBirney AR and Murase T (1984) Rheological properties of magmas. *Annual Review of Earth and Planetary Sciences* 12: 337–357.

McFarlane EA and Drake MJ (1990) Element partitioning and the early thermal history of the Earth. In: Newsom HE and Jones JH (eds.) *Origin of the Earth*, pp. 135–150. New York: Oxford University Press.

McFarlane EA, Drake MJ, and Rubie DC (1994) Element partitioning between Mg-perovskite, magnesiowustite, and silicate melt at conditions of the Earth's mantle. *Geochimica et Coscochimica Acta* 58: 5161–5172.

McGeary RK (1961) Mechanical packing of spherical particles. *Journal of the American Ceramic Society* 44: 513–522.

McKenzie D (1984) The generation and compaction of partially molten rock. *Journal of Petrology* 25: 713–765.

McKenzie D and Bickle MJ (1988) The volume and composition of melt generated by extension of the lithosphere. *Journal of Petrology* 29: 625–679.

Mei S, Bai W, Hiraga T, and Kohlstedt DL (2002) Influence of melt on the creep behavior of olivine-basalt aggregates under hydrous conditions. *Earth and Planetary Science Letters* 201: 491–507.

Mei S and Kohlstedt DL (2000a) Influence of water on plastic deformation of olivine aggregates 1. Diffusion creep regime. *Journal Geophysical Research* 105: 21457–21469.

Mei S and Kohlstedt DL (2000b) Influence of water on plastic deformation of olivine aggregates 2. Dislocation creep regime. *Journal of Geophysical Research* 105: 21471–21481.

Melosh HJ (1990) Giant impacts and the thermal state of the early Earth. In: Newsom HE and Jones JH (eds.) *Origin of the Earth*, pp. 69–83. New York: Oxford University Press.

Miller GH, Stolper EM, and Ahrens TJ (1991a) The equation of state of a molten komatiite, 1. Shock wave compression to 36 GPa. *Journal of Geophysical Research* 96: 11831–11848.

Miller GH, Stolper EM, and Ahrens TJ (1991b) The equation of state of a molten komatiite, 2, Application to komatiite petrogenesis and the Hadean mantle. *Journal of Geophysical Research* 96: 11849–11864.

Mooney M (1951) The viscosity of a concentrated suspension of spherical particles. *Journal of Colloid Science* 6: 162–170.

Morris S and Canright D (1984) A boundary layer analysis of Bénard convection in a fluid of strongly temperature dependent viscosity. *Physics of the Earth and Planetary Interiors* 36: 355–373.

Mosenfelder JL, Asimow PD, Frost DJ, Rubie DC, and Ahrens TJ (2009) The $MgSiO_3$ system at high pressure: Thermodynamic properties of perovskite, postperovskite, and melt from global inversion of shock and static compression data. *Journal of Geophysical Research* 114. http://dx.doi.org/10.1029/2008JB005900.

Mostefaoui S, Lugmair GW, and Hoppe P (2005) Fe-60: A heat source for planetary differentiation from a nearby supernova explosion. *Astrophysical Journal* 625: 271–277.

Murakami M and Bass JD (2011) Evidence of denser $MgSiO_3$ glass above 133 gigapascal (GPa) and implications for remnants of ultradense silicate melt from a deep magma ocean. *Proceedings of the National Academy of Sciences* 108: 17286–17289.

Murase T and McBirney AR (1973) Properties of some common igneous rocks and their melts at high temperatures. *Geological Society of America Bulletin* 84: 3563–3593.

Murray JD (1965) On the mathematics of fluidization, Part I. Fundamental equations and wave propagation. *Journal of Fluid Mechanics* 21: 465–493.

Nakazawa K, Mizuno H, Sekiya M, and Hayashi C (1985) Structure of the primordial atmosphere surrounding the early Earth. *Journal of Geomagnetism and Geoelectricity* 37: 781–799.

Newsom HE and Taylor SR (1989) Geochemical implications of the formation of the Moon by a single giant impact. *Nature* 338: 29–34.

Nicolas A and Ildefonse B (1996) Flow mechanism and viscosity in basaltic magma chambers. *Geophysical Research Letters* 23: 2013–2016.

Nicolis G and Prigogine I (1977) *Self-Organization in Non-Equilibrium Systems*. New York: Wiley.

Niemela JJ, Skrbek L, Sreenivasan KR, and Donnelly RJ (2000) Turbulent convection at very high Rayleigh numbers. *Nature* 404: 837–840.

Nomura R, Ozawa H, Tateno S, et al. (2011) Spin crossover and iron-rich silicate melt in the Earth's deep mantle. *Nature* 473: 199–203.

Ohtani E (1985) The primordial terrestrial magma ocean and its implication for stratification of the mantle. *Physics of the Earth and Planetary Interiors* 38: 70–80.

Ohtani E (2009) Melting relations and the equation of state of magmas at high pressure: Application to geodynamics. *Chemical Geology* 265: 279–288.

Ohtani E and Maeda M (2001) Density of basaltic melt at high pressure and stability of the melt at the base of the lower mantle. *Physics of the Earth and Planetary Interiors* 193: 69–75.

Ohtani E and Sawamoto H (1987) Melting experiment on a model chondritic mantle composition at 25 GPa. *Geophysical Research Letters* 14: 733–736.

Persikov ES, Zharikov VA, Bukhtiyarov PG, and Polskoy SF (1997) The effect of volatiles on the properties of magmatic melts. *European Journal of Mineralogy* 2: 621–642.

Pierazzo E, Vickery AM, and Melosh HJ (1997) A reevaluation of impact melt production. *Icarus* 127: 408–423.

Pinkerton H and Sparks RSJ (1978) Field measurements of the rheology of lava. *Nature* 276: 383–385.

Poe BT, McMillan PF, Rubie DC, Chakraborty S, Yarger J, and Diefenbacher J (1997) Silicon and oxygen self-diffusivities in silicate liquids measured to 15 gigapascals and 2800 kelvin. *Science* 276: 1245–1248.

Presnall DC, Weng Y-H, Milholland CS, and Walter MJ (1998) Liquidus phase relations in the system $MgO–MgSiO_3$ at pressures up to 25 GPa – Constraints on crystallization of a molten Hadean mantle. *Physics of the Earth and Planetary Interiors* 107: 83–95.

Priestly CHB (1959) *Turbulent Transfer in the Lower Atmosphere*. Chicago, IL: University of Chicago Press.

Qin LP, Dauphas N, Wadhwa M, et al. (2008) Rapid accretion and differentiation of iron meteorite parent bodies inferred from 182Hf-182W chronometry and thermal modeling. *Earth and Planetary Science Letters* 273: 94–104.

Raizer Yu P (1960) Condensation of a cloud of vaporized matter expanding in vacuum. *Soviet Physics JETP (English Translation)* 10: 1229–1235.

Reese CC and Solomatov VS (2006) Fluid dynamics of local martian magma oceans. *Icarus* 184: 102–120.

Reese CC, Solomatov VS, and Orth CP (2007a) Mechanisms for cessation of magmatic resurfacing on Venus. *Journal of Geophysical Research* 112. http://dx.doi.org/10.1029/2006JE002782.

Reese CC, Solomatov VS, and Orth CP (2007b) Interaction between local magma ocean evolution and mantle dynamics on Mars. In: Foulger GR and Jurdy DM (eds.) *Plates, Plumes, and Planetary Processes*, pp. 913–932. Geological Society of America.

Righter K (2003) Metal-silicate partitioning of siderophile elements and core formation in the early Earth. *Annual Review of Earth and Planetary Sciences* 31: 135–174.

Righter K (2011) Prediction of metal–silicate partition coefficients for siderophile elements: An update and assessment of PT conditions for metal–silicate equilibrium during accretion of the Earth. *Earth and Planetary Science Letters* 304: 158–167.

Righter K and Drake MJ (1997) Metal-silicate equilibrium in a homogeneously accreting Earth: New results for Re. *Earth and Planetary Science Letters* 146: 541–553.

Righter K, Drake MJ, and Yaxley G (1997) Prediction of siderophile element metal-silicate partition coefficients to 20 GPa and 2800 °C: The effects of pressure, temperature, oxygen fugacity, and silicate and metallic melt compositions. *Physics of the Earth and Planetary Interiors* 100: 115–134.

Ringwood AE (1990) Earliest history of the Earth–Moon system. In: Newsom NE and Jones JH (eds.) *Origin of the Earth*, pp. 101–134. New York: Oxford University Press.

Ringwood AE and Kesson SE (1976) A dynamic model for mare basalt petrogenesis. In: *Proceedings of the 7th Lunar Planetary Science Conference*, pp. 1697–1722.

Robson GR (1967) Thickness of Etnean lavas. *Nature* 216: 251–252.

Roscoe R (1952) The viscosity of suspensions of rigid spheres. *British Journal of Applied Physics* 3: 267–269.

Rubie DC, Melosh HJ, Reid JE, Liebske C, and Righter K (2003) Mechanisms of metal–silicate equilibration in the terrestrial magma ocean. *Earth and Planetary Science Letters* 205: 239–255.

Rudman M (1992) Two-phase natural convection: Implications for crystal settling in magma chambers. *Physics of the Earth and Planetary Interiors* 72: 153–172.

Rutter EH and Neumann DHK (1995) Experimental deformation of partially molten Westerly granite under fluid-absent conditions, with implications for the extraction of granitic magmas. *Journal of Geophysical Research* 100: 15697–15715.

Ryerson FJ, Weed HC, and Piwinskii AJ (1988) Rheology of subliquidus magmas: I. Picritic compositions. *Journal of Geophysical Research* 93: 3421–3436.
Saar MO, Manga M, Cashman KV, and Fremouw S (2001) Numerical models of the onset of yield strength in crystal-melt suspensions. *Earth Planet Science Letters* 187: 367–379.
Safronov VS (1964) The primary inhomogeneities of the Earth's mantle. *Tectonophysics* 1: 217–221.
Safronov VS (1978) The heating of the Earth during its formation. *Icarus* 33: 3–12.
Scarfe CM and Takahashi E (1986) Melting of garnet peridotite to 13 GPa and the early history of the upper mantle. *Nature* 322: 354–356.
Scherstén A, Elliott T, Hawkesworth C, et al. (2006) Hf-W evidence for rapid differentiation of iron meteorite parent bodies. *Earth and Planetary Science Letters* 241: 530–542.
Sears WD (1993) Tidal dissipation and the giant impact origin for the Moon. *Lunar and Planetary Science Conference* 23: 1255–1256.
Shankland TJ, Nitsan U, and Duba AG (1979) Optical absorption and radiative heat transport in olivine at high temperatures. *Journal of Geophysical Research* 84: 1603–1610.
Shaw HR (1969) Rheology of basalt in the melting range. *Journal of Petrology* 10: 510–535.
Shaw HR (1972) Viscosities of magmatic silicate liquids: An empirical method of prediction. *American Journal of Science* 272: 870–893.
Shaw HR, Wright TL, Peck DL, and Okamura R (1968) The viscosity of basaltic magma: An analysis of field measurements in Makaopuhi lava lake, Hawaii. *American Journal of Science* 266: 225–264.
Shraiman BI and Siggia ED (1990) Heat transport in high-Rayleigh-number convection. *Physical Review A* 42: 3650–3653.
Shukolyukov A and Lugmair GW (1993) Live iron-60 in the early solar system. *Science* 259: 1138–1142.
Siebert J, Badro J, Antonangeli D, and Ryerson FJ (2012) Metal silicate partitioning of Ni and Co in a deep magma ocean. *Earth and Planetary Science Letters* 321–322: 189–197.
Siggia ED (1994) High Rayleigh number convection. *Annual Review of Fluid Mechanics* 26: 137–168.
Sleep NH (2000) Evolution of the mode of convection within terrestrial planets. *Journal of Geophysical Research* 105. http://dx.doi.org/10.1029/2000JE001240.
Smith DM, Eady JA, Hogan LM, and Irwin DW (1991) Crystallization of a faceted primary phase in a stirred slurry. *Metallurgical Transactions A* 22: 575–584.
Smrekar SE, Stofan ER, Mueller N, et al. (2010) Recent hotspot volcanism on Venus from VIRTIS emissivity data. *Science* 328: 605–608.
Solomatov VS (1995a) Scaling of temperature- and stress-dependent viscosity convection. *Physics of Fluids* 7: 266–274.
Solomatov VS (1995b) Batch crystallization under continuous cooling: Analytical solution for diffusion limited crystal growth. *Journal of Crystal Growth* 148: 421–431.
Solomatov VS (2000) Fluid dynamics of a terrestrial magma ocean. In: Canup RM and Righter K (eds.) *Origin of the Earth and Moon*, pp. 323–338. Tucson, AZ: University of Arizona Press.
Solomatov VS and Moresi L-N (2000) Scaling of time-dependent stagnant lid convection: Application to small-scale convection on the Earth and other terrestrial planets. *Journal of Geophysical Research* 105: 21795–21818.
Solomatov VS, Olson P, and Stevenson DJ (1993) Entrainment from a bed of particles by thermal convection. *Earth and Planetary Science Letters* 120: 387–393.
Solomatov VS and Reese CC (2008) Grain size variations in the Earth's mantle and the evolution of primordial chemical heterogeneities. *Journal of Geophysical Research* 113. http://dx.doi.org/10.1029/2007JB005319.
Solomatov VS and Stevenson DJ (1993a) Suspension in convective layers and style of differentiation of a terrestrial magma ocean. *Journal of Geophysical Research* 98: 5375–5390.
Solomatov VS and Stevenson DJ (1993b) Nonfractional crystallization of a terrestrial magma ocean. *Journal of Geophysical Research* 98: 5391–5406.
Solomatov VS and Stevenson DJ (1993c) Kinetics of crystal growth in a terrestrial magma ocean. *Journal of Geophysical Research* 98: 5407–5418.
Sonett CP, Colburn DS, and Schwartz K (1968) Electrical heating of meteorite parent bodies and planets by dynamo induction from a pre-main sequence T Tauri solar wind. *Nature* 219: 924–926.
Soo SL (1967) *Fluid Dynamics of Multiphase Systems*. Waltham: Blaisdell.
Sparks RS, Huppert HE, Koyaguchi T, and Hallworth MA (1993) Origin of modal and rhythmic igneous layering by sedimentation in a convecting magma chamber. *Nature* 361: 246–249.
Srinivasan G, Goswami JN, and Bhandari N (1999) ^{26}Al in eucrite Piplia Kalan: Plausible heat source and formation chronology. *Science* 284: 1348–1350.
Stevenson DJ (1981) Models of the Earth's core. *Science* 214: 611–619.
Stevenson DJ (1987) Origin of the Moon – The collision hypothesis. *Annual Review of Earth and Planetary Sciences* 15: 271–315.
Stevenson DJ (1990) Fluid dynamics of core formation. In: Newsom HE and Jones JH (eds.) *Origin of the Earth*, pp. 231–249. New York: Oxford University Press.
Stevenson DJ (2008) A planetary perspective on the deep Earth. *Nature* 45: 261–265.
Stishov SM (1988) Entropy, disorder, melting. *Soviet Physics Uspekhi* 31: 52–67.
Stixrude L and Karki B (2005) Structure and freezing of $MgSiO_3$ liquid in Earth's lower mantle. *Science* 14: 297–299.
Thomas CW, Liu Q, Agee CB, Asimow PD, and Lange RA (2012) Multi-technique equation of state for Fe_2SiO_4 melt and the density of Fe-bearing silicate melts from 0 to 161 GPa. *Journal of Geophysical Research* 117. http://dx.doi.org/10.1029/2012JB009403.
Thompson C and Stevenson DJ (1988) Gravitational instabilities in 2-phase disks and the origin of the Moon. *Astrophysical Journal* 333: 452–481.
Thomson W (1864) On the secular cooling of the Earth. *Transactions of Royal Society of Edinburgh* 23: 157–169.
Tomkins AG, Weinberg RF, Schaefer BF, and Langendam A (2013) Disequilibrium melting and melt migration driven by impacts: Implications for rapid planetesimal core formation. *Geochimica et Cosmochimica Acta* 100: 41–59.
Tonks WB and Melosh HJ (1990) The physics of crystal settling and suspension in a turbulent magma ocean. In: Newsom HE and Jones JH (eds.) *Origin of the Earth*, pp. 151–174. New York: Oxford University Press.
Tonks WB and Melosh HJ (1992) Core formation by giant impacts. *Icarus* 100: 326–346.
Tonks WB and Melosh HJ (1993) Magma ocean formation due to giant impacts. *Journal of Geophysical Research* 98: 5319–5333.
Touboul M, Puchtel IS, and Walker RJ (2012) ^{182}W evidence for long-term preservation of early mantle differentiation products. *Science* 335: 1065–1069.
Turcotte DL and Schubert G (2002) *Geodynamics*, 2nd edn. New York: Cambridge University Press.
Urey HC (1955) The cosmic abundances of potassium, uranium, and thorium and the heat balances of the Earth, the Moon, and Mars. *Proceedings of the National Academy of Sciences of the United States of America* 41: 127–144.
van der Molen I and Paterson MS (1979) Experimental deformation of partially-melted granite. *Contributions to Mineralogy and Petrology* 70: 299–318.
Voorhees PW (1992) Ostwald ripening of two-phase mixtures. *Annual Review of Materials Science* 22: 197–215.
Walker D, Powell MA, Lofgren GE, and Hays JF (1978) Dynamic crystallization of a eucrite basalt. In: *Proceedings of the 9th Lunar and Planetary Science Conference,* pp. 1369–1391.
Walter MJ, Nakamura E, Trønnes RG, and Frost DJ (2004) Experimental constraints on crystallization differentiation in a deep magma ocean. *Geochimica et Cosmochimica Acta* 68: 4267–4284.
Walter MJ and Trønnes RG (2004) Early Earth differentiation. *Earth and Planetary Science Letters* 225: 253–269.
Warren PH (1985) The magma ocean concept and lunar evolution. *Annual Review of Earth and Planetary Sciences* 13: 201–240.
Weidenschilling SJ, Spaute D, Davis DR, Marzari F, and Ohtsuki K (1997) Accretional evolution of a planetesimal swarm. 2. The terrestrial zone. *Icarus* 128: 429–455.
Weinstein SA, Yuen DA, and Olson PL (1988) Evolution of crystal-settling in magma-chamber convection. *Earth and Planetary Science Letters* 87: 237–248.
Wetherill GW (1975) Radiometric chronology of the early solar system. *Annual Review of Nuclear Science* 25: 283–328.
Wetherill GW (1985) Occurrence of giant impacts during the growth of the terrestrial planets. *Science* 228: 877–879.
Wetherill GW (1990) Formation of the Earth. *Annual Review of Earth and Planetary Sciences* 18: 205–256.
Willis GE and Deardorff JW (1974) A laboratory model of the unstable planetary boundary layer. *Journal of Atmospheric Science* 31: 1297–1307.
Wood JA (1975) Lunar petrogenesis in a well-stirred magma ocean. In: *Proceedings of the 6th Lunar Science Conference,* pp. 1087–1102.
Wood JA, Dickey JS, Marvin UB, and Powell BN (1970) Lunar anorthosites and a geophysical model of the moon. In: Levinson AA (ed.) *Proceedings of the Apollo 11 Lunar Science Conference*, pp. 965–988. New York: Pergamon.
Wright K and Price GD (1993) Computer simulation of defects and diffusion in perovskites. *Journal of Geophysical Research* 98: 22245–22253.
Yamazaki D and Karato S-I (2001) Some mineral physics constraints on the rheology and geothermal structure of Earth's lower mantle. *American Mineralogist* 86: 385–391.
Yamazaki D, Kato T, Yurimoto H, Ohtani E, and Toriumi M (2000) Silicon self-diffusion in $MgSiO_3$ perovskite at 25 GPa. *Physics of the Earth and Planetary Interiors* 119: 299–309.

Yin Q, Jacobsen SB, Yamashita K, Blichert-Toft J, Telouk P, and Albarède F (2002) A short timescale for terrestrial planet formation from Hf–W chronometry of meteorites. *Nature* 418: 949–952.

Yoshino T, Walter MJ, and Katsura T (2003) Core formation in planetesimals triggered by permeable flow. *Nature* 422: 154–157.

Zahnle K, Arndt N, Cockell C, et al. (2007) Emergence of a habitable planet. *Space Science Reviews* 129: 35–78.

Zahnle KJ, Kasting JF, and Pollack JB (1988) Evolution of a steam atmosphere during Earth's accretion. *Icarus* 74: 62–97.

Zaranek SE and Parmentier EM (2004) Convective cooling of an initially stably stratified fluid with temperature-dependent viscosity: Implications for the role of solid-state convection in planetary evolution. *Journal of Geophysical Research* 109. http://dx.doi.org/10.1029/2003JB002462.

Zel'dovich Ya B and Raizer Yu P (2002) *Physics of Shock Waves and High-Temperature Hydrodynamic Phenomena*. Mineola, NY: Dover Publications.

Zerr A and Boehler R (1993) Melting of $(Mg,Fe)SiO_3$-perovskite to 625 kilobars: Indication of a high melting temperature in the lower mantle. *Science* 262: 553–555.

Zerr A and Boehler R (1994) Constraints on the melting temperature of the lower mantle from high-pressure experiments on MgO and magnesiowustite. *Nature* 371: 506–508.

Zerr A, Diegeler A, and Boehler R (1998) Solidus of Earth's deep mantle. *Science* 281: 243–246.

Zhang J and Herzberg CT (1994) Melting experiments on anhydrous peridotite KLB-1 from 5.0 to 22.5 GPa. *Journal of Geophysical Research* 99: 17729–17742.